DOKUZ EYLÜL UNIVERSITY
GRADUATE SCHOOL OF NATURAL AND APPLIED SCIENCES

SYNTHESIS OF HIGH QUALITY GRAPHENE AND INVESTIGATION OF THE USE OF GRAPHENE BASED MATERIALS FOR ENERGY STORAGE APPLICATIONS

by
Eyyüp Can DOLUEL

January, 2022
İZMİR

SYNTHESIS OF HIGH QUALITY GRAPHENE AND INVESTIGATION OF THE USE OF GRAPHENE BASED MATERIALS FOR ENERGY STORAGE APPLICATIONS

A Thesis Submitted to the
Graduate School of Natural and Applied Sciences of Dokuz Eylül University
In Partial Fulfillment of the Requirements for the Degree of Master of Science in Metallurgical and Materials Engineering

by
Eyyüp Can DOLUEL

January, 2022
İZMİR

M.Sc THESIS EXAMINATION RESULT FORM

We have read the thesis entitled **"SYNTHESIS OF HIGH QUALITY GRAPHENE AND INVESTIGATION OF THE USE OF GRAPHENE BASED MATERIALS FOR ENERGY STORAGE APPLICATIONS"** completed by **EYYÜP CAN DOLUEL** under supervision of **ASSOC. PROF. DR. METİN YURDDAŞKAL** and we certify that in our opinion it is fully adequate, in scope and in quality, as a thesis for the degree of Master of Science.

.....

Assoc. Prof. Dr. Metin YURDDAŞKAL

Supervisor

.....

Prof. Dr. Hülya DURMUŞ

Jury Member

.....

Assist. Prof. Dr. Serdar YILDIRIM

Jury Member

Prof. Dr. Okan FISTIKOĞLU

Director

Graduate School of Natural and Applied Sciences

ACKNOWLEDGEMENT

I would like to thank everyone for their sincere support on this stressful but enjoyable journey that I have embarked on to obtain my master's degree.

Firstly, I would like to tell my interior appreciation to my advisor, Assoc. Prof. Dr. Metin YURDDAŞKAL, for his constructive ideas, supervision, support, understanding, contributions, and encouragement during my thesis.

I would also like to thank my committee members, Prof. Dr. Hülya DURMUŞ and Assist. Prof. Dr. Serdar YILDIRIM for reviewing my thesis and offering precious suggestions and sharing their visions.

I would like to present my special thanks to Dokuz Eylül University Electronic Materials Production and Application Center and its staff for the resources they enable for me. Also, I would like to thank Assoc. Prof. Dr. Mustafa EROL, Assoc. Prof. Dr. Tuncay DİKİCİ, Dr. Hilmiye Deniz ERTUĞRUL UYGUN, and Uğur KARTAL for their precious help, support, and nice friendship.

Finally, and most importantly, my family's support and belief in me has always motivated me. My mother Canan DOLUEL and my father Necmi DOLUEL deserve the greatest thanks for their love and support, as they are always by my side. I should also thank my sister Nida DOLUEL for their endless support to me.

Eyyüp Can DOLUEL

SYNTHESIS OF HIGH QUALITY GRAPHENE AND INVESTIGATION OF THE USE OF GRAPHENE BASED MATERIALS FOR ENERGY STORAGE APPLICATIONS

ABSTRACT

With the ever-increasing need for energy, the storage of energy is as important as its production. Especially with the decrease in fossil fuel resources in the world, the rate of use of electrical energy is increasing very rapidly. Renewable energy sources such as solar energy and wind energy are used for the production of electrical energy. Another issue as important as the production of electrical energy is the efficient storage of the produced energy. Among the new generation energy storage systems, lithium-ion batteries are the most efficient. Within the scope of this thesis, studies have been carried out to increase the efficiency of the anode, which is one of the most important components of the system, with graphene, a new generation material, in order to make lithium-ion batteries more efficient. Graphene was produced by different methods and its anodic performances were evaluated. The produced graphene samples were analyzed by X-ray diffractometry, scanning electron microscopy, X-ray photoelectron spectroscopy, and Raman spectroscopy analysis. Anode performances of graphene samples were investigated by the electrochemical analysis method. The results showed that the produced graphene samples are suitable to be used for the anode material. At the same time, the results also revealed that the produced graphene anode structures are suitable for use in lithium-ion batteries, which are frequently used in daily life.

Keywords: Graphene, energy storage, graphene oxide, Li-ion battery, characterization

YÜKSEK KALİTELİ GRAFEN SENTEZİ VE ENERJİ DEPOLAMA UYGULAMALARI İÇİN GRAFEN BAZLI MALZEMELERİN KULLANIMININ ARAŞTIRILMASI

ÖZ

Her geçen gün artan enerji ihtiyacı ile birlikte enerjinin üretimi kadar depolanması da oldukça önem arz etmektedir. Özellikle dünya üzerindeki fosil yakıt kaynaklarının azalmaya başlaması ile birlikte elektrik enerjisi kullanım oranı oldukça hızlı artmaktadır. Elektrik enerjisinin üretimi için güneş enerjisi, rüzgar enerjisi gibi yenilenebilir enerji kaynaklarından faydalanılmaktadır. Elektrik enerjisinin üretimi kadar önemli olan bir diğer konu ise üretilen enerjisinin verimli bir şekilde depolanabilmesidir. Yeni nesil enerji depolama sistemleri arasında en verimli olanı lityum iyon pillerdir. Bu tez kapsamında lityum iyon pillerin daha verimli hale getirilmesi için sistemin en önemli bileşenlerinden olan anodun, yeni nesil bir malzeme olan grafen ile verimliliğinin arttırılması üzerine çalışmalar yapılmıştır. Farklı yöntemlerle grafen üretimi yapılmış olup anodik performansları değerlendirilmiştir. Üretilen grafen numuneleri X-ışını difraktometresi, taramalı elektron mikroskobu, X-ışını fotoelektron spektroskopisi, Raman spektroskopisi analizleri ile incelenmiştir. Grafen numunelerin anot performansları ise elektrokimyasal analiz yöntemiyle incelenmiştir. Sonuçlar, üretilen grafen numunelerin anot malzemesi için kullanılmak üzere uygun olduğunu göstermiştir. Aynı zamanda sonuçlar, üretilen grafen anot yapıların günlük hayatta sıklıkla kullanılan lityum iyon pillerde kullanımının uygun olduğunu da ortaya koymuştur.

Anahtar kelimeler: Grafen, enerji depolama, grafen oksit, Li-iyon pil, karakterizasyon

CONTENTS

Page

M.Sc THESIS EXAMINATION RESULT FORM ……...ii

ACKNOWLEDGEMENT iii

ABSTRACT iv

ÖZ v

LIST OF FIGURES ix

LIST OF TABLES xi

CHAPTER ONE - INTRODUCTION 1

1.1 Background 1

1.2 Organization of the Thesis 3

CHAPTER TWO - THEORETICAL BACKGROUND 5

2.1 Graphene 5

2.1.1 Graphene Types 7

2.1.2 Graphene Production Methods 8

2.1.2.1 Mechanical Exfoliation 10

2.1.2.2 Liquid-phase Exfoliation (LPE) 10

2.1.2.3 Chemical vapor deposition (CVD) 11

2.1.2.4 Reduction of Graphene Oxide 12

2.1.3 Application of Graphene 14

2.1.3.1 Energy 14

2.1.3.2 Wearable Technologies 15

2.1.3.3 Wastewater Management 17

2.1.3.4 Medical Applications 18
2.1.3.5 Composite Industry 19
2.2 Battery Systems 20
2.2.1 Battery Types 20
2.2.1.1 Lithium-Ion Battery 23
2.2.2 Anode Materials 29
2.2.2.1 Graphene Anode Materials 30

CHAPTER THREE - LITERATURE REVIEW 32

3.1 Graphene Anode Materials for Lithium-Ion Batteries 32

CHAPTER FOUR - EXPERIMENTAL PROCEDURE 35

4.1 Purpose 35
4.2 Materials 35
4.3 Methods 36
4.4 Materials Characterization 41
4.4.1 X-ray Diffraction 41
4.4.2 Scanning Electron Microscopy 42
4.4.3 X-Ray Photoelectron Spectroscopy 43
4.4.4 Raman Spectroscopy 44
4.4.5 Electrochemical Measurements 45

CHAPTER FIVE - RESULTS AND DISCUSSION 47

5.1 Structural Properties 47

5.2 Morphological Properties 49

5.3 Chemical Properties 51

5.4 Raman Analysis 54

5.5 Electrochemical Measurements 55

CHAPTER SIX - CONCLUSION AND FUTURE WORKS 58

REFERENCES 59

LIST OF FIGURES

Page

Figure 2.1 Scheme showing graphene can be wrapped up to form 0D fullerenes, wrapped up to form 1D CNTs, or stacked up to form 3D graphite 5
Figure 2.2 Basic graphene forms 8
Figure 2.3 Chart of basic graphene production methods 9
Figure 2.4 Mechanical exfoliation method 10
Figure 2.5 A representative illustration of the LPE method 11
Figure 2.6 The representative illustration of graphene production by CVD method. 12
Figure 2.7 The representative illustration that explains the basic principle of the reduction of graphene oxide method 13
Figure 2.8 Reduced graphene oxide production flowchart 13
Figure 2.9 The most well-known rGO fabrication methods 13
Figure 2.10 The illustration representing the graphene-based energy conversion and storage systems 15
Figure 2.11 Brief illustration of the graphene-based sensor platform for health monitoring 17
Figure 2.12 (a) Different types of graphene-based membranes, (b) Water separation membrane 18
Figure 2.13 Applications of graphene-based materials in medical 19
Figure 2.14 The basic battery system 20
Figure 2.15 Schematic illustration of representative rechargeable batteries and their applications 21
Figure 2.16 The number of various metals in the world (a) and their average sales prices (b) 24
Figure 2.17 The theoretical and experimental values of electrical potential and capacity of varios materials used in Li-ion battery system (LCO: lithium cobalt oxide, LMO: lithium manganese oxide, NCM: nickel cobalt manganese oxide, NCA: nickel cobalt aluminum oxide, LCP: lithium cobalt phosphate, LFP: lithium iron phosphate, LFSF: lithium iron fluorosilicate, LTS: lithium titanium sulfide) 25
Figure 2.18 Lithium-ion battery working principle 26

Figure 2.19 Electrochemical potentials of compounds that give reversible reactions with lithium due to metallic lithium 27
Figure 2.20 The structures of $LiCoO_2$ with a layered structure, $LiMn_2O_4$ with a spinel structure and $LiFePO_4$ with an olivine structure 28
Figure 4.1 The image of (a) the triple electrode system and (b) the sample image of the prepared anodes 40
Figure 4.2 X-Ray Diffractometer analysis device, Thermoscientific ARL X'TRA .. 41
Figure 4.3 SEM analysis device, Zeiss-Gemini 43
Figure 4.4 XPS analysis device, Thermo Scientific K-Alpha 44
Figure 4.5 Renishaw Raman Spectroscopy device 45
Figure 4.6 PalmSens 3 potentiostat/galvanostat device 46
Figure 5.1 XRD graphs of graphite and graphene samples 48
Figure 5.2 Sem images of graphite and graphene samples 50
Figure 5.3 XPS spectra of graphite and graphene samples 52
Figure 5.4 Raman graphs of graphite and graphene samples 54
Figure 5.5 CV graphs of graphite and graphene samples 56
Figure 5.6 EIS analysis graphs of samples 57

LIST OF TABLES

Page

Table 4.1 Properties of materials used in experimental studies 36
Table 4.2 Codes of all produced samples..... 39
Table 4.3 Working electrode (anode) slurry recipe 40
Table 5.1 2θ diffraction angles and maximum intensities of XRD graphs 48
Table 5.2 The binding energies, FWHM values, and detailed chemical properties of the peaks of the elements in graphite and graphene samples 53
Table 5.3 I_{2D} and I_G data and I_{2D}/I_G ratios of samples..... 55

CHAPTER ONE
INTRODUCTION

1.1 Background

Today, with the increasing energy need around the world, fossil fuels such as coal, oil and natural gas, which are our main energy resources, are consumed rapidly. The rapid consumption of fossil resources causes serious crises and environmental pollution. In the 2030s, the global total oil demand is expected to reach 1500 million tons. This energy demand creates pressure to meet their energy needs and creates an obligation on countries to turn to alternative energy sources (Bruce et al., 2011; Y. Li et al., 2014). Important studies are carried out on renewable and sustainable energy to overcome these problems. In the past years, a lot of effort has been made and important studies have been carried out to collect and store sustainable clean energy (Johansson, 2013). With the development of materials science, nanoscience and nanotechnology, tremendous work is being done for the need for clean sustainable energy. Thanks to these studies, clean energy technologies have become more competitive against fossil fuels. Today, with the developing technology, the production of electrical energy from renewable energy sources such as solar and wind energies is in increasing demand(Armand et al., 2008). However, energy efficiency in these renewable energy sources is not always at the same rate. Therefore, these energies must be stored efficiently. The task of electrical energy storage devices is to store energy efficiently and to provide uninterrupted electrical energy to the electrical network. Since energy storage devices are needed in all electrical devices, there is an intense need for the development of energy storage devices (Bradley & Frank, 2009; Datta et al., 2011).

Rechargeable lithium-ion batteries are the leading chemical energy storage technologies. Lithium-ion batteries were first produced commercially by Sony in 1991 and emerged as the rechargeable batteries of the future (W. Wang & Kumta, 2010). Lithium-ion batteries have been desired to be used in electrical devices and stationary power systems, and are now used as power sources in areas such as digital camera, laptop computers, telephone and video camera batteries(Gu et al., 2010; Tarascon &

Armand, 2001). In addition to these applications, it is clear that in the near future, vehicles running on fossil fuels will be completely replaced by vehicles powered by electricity. Considering all these needs and the decreasing lithium resources day by day, it is very important to provide high energy and power density, fast charging capability and long discharge times from lithium-ion batteries in terms of meeting the required need (McDowell et al., 2013).

Lithium-ion batteries consist of an anode (negative electrode) and a cathode (positive electrode). These two electrodes can reversibly contain lithium in its ionic form. In lithium-ion batteries, metal oxides containing lithium ($LiCoO_2$, $LiNiO_2$, $LiMnO_2$, $LiMn_2O_4$, $LiFePO_4$, and LiV_3O_8 etc.) are generally used as the cathode material, while carbon-based materials (graphite, active carbon, carbon nanotube, carbon black, amorphous carbon, and graphene, etc.) are used as the anode material (Orsini et al., 1999). Lithium metal was used before the discovery of graphite anode materials. However, the possibility of thermal runaway caused by internal short circuits triggered by the formation of lithium dendrites has been a longstanding issue. Later, it was proposed to use graphite material with a suitable structure for the incorporation of lithium ions between the layers of the anode material in rechargeable lithium-ion batteries (Armand & Touzain, 1977). Graphite has hitherto been used as the main anode material for commercial lithium-ion batteries due to its layered structure suitable for lithium intercalation, low operating potential and remarkable interfacial stability. However, the most important disadvantage is that the intercalation capacity of lithium ions in graphite is limited to 372 mAh/g in relation to the LiC_6 stoichiometry. Many studies have been carried out to increase this value by changing the crystallinity, microstructure and micromorphology of the carbonaceous material (Endo et al., 2000; Mabuchi et al., 1995; Ruland, 2004).

In recent years, there has been a great interest in graphene material as an anode material that can be used instead of graphite, thanks to its 2D structure that provides twice the capacity. Graphene; It has opened a new era in technology, thanks to its 2-dimensional, honeycomb lattice and single-layer structure being different from other

carbon allotropes (J. Liu et al., 2013). Its two-dimensional structure means that each atom behaves as a surface atom (Kucinskis et al., 2013).

Graphene has high mechanical strength (Young modulus ~1100Gpa), electrical conductivity (~104 Ω-1 cm-1), thermal conductivity (~3000 W/mK), large specific surface area (2630 m2 g-1) and high It has properties such as chemical stability. These properties make graphene a promising material in many applications such as electronics, energy storage and conversion, sensors, solar cells and catalysts (Allen et al., 2009; S. Guo & Dong, 2011; Yoo & Zhou, 2011). Thanks to all these features, graphene is a very important material that can be used instead of graphite in lithium-ion batteries and can provide extremely efficient results.

1.2 Organization of the Thesis

Within the scope of this thesis, graphene was produced by different methods and the use of the produced graphene samples as anodes in lithium-ion batteries was investigated. The aim of the thesis is to compare the anodic performance of graphene structures produced by different methods and to reveal the production method-performance relationship.

Chapter 1, a brief description of graphene and energy storage systems is given. At the same time, the organization of the thesis is presented in this section.

In the chapter 2, graphene, the importance of graphene, graphene derivatives, graphene production methods, application areas of graphene, energy storage systems, lithium-ion batteries, and the use of graphene in energy storage systems are explained in detail.

In Chapter 3, literature review about graphene anodes is presented in detail.

Experimental studies carried out within the scope of the thesis are presented in chapter 4. Graphene production, application as anode and characterization methods are

given in this section. The list of names and properties of the materials used in production is also presented. X-ray diffraction (XRD) and Raman analysis for structural analysis, scanning electron microscopy (SEM) for morphology analysis, X-ray photoelectron spectroscopy (XPS) for chemical analysis, cyclic voltammetry (CV) for electrochemical analysis, and electrochemical Impedance (EIS) details are explained in this section.

In Chapter 5, the results and discussion of the characterization processes are presented. The results of some analyzes have been supported with graphics and interpreted more efficiently.

In the last chapter 6, general conclusions and future plans are presented.

CHAPTER TWO
THEORETICAL BACKGROUND

2.1 Graphene

Graphene is a sp^2 bonded 2D allotrope of carbon consisting of one or a few graphitic layers. Graphene is considered a unique material due to its properties such as outstanding electrical and thermal conductivity, high charge carrier density and carrier mobility, high optical transmittance, and high mechanical strength (Choi et al., 2010; Geim & Kim, 2008; Geim & Novoselov, 2007; Lee et al., 2008; Nair et al., 2008). Thanks to these features, it has attracted great interest to be used in fields such as new generation composite, electronic and photonic materials. In general, the basic building block of carbon nanostructures is a single graphitic layer with a hexagonal honeycomb structure consisting of carbon atoms bonded to each other by covalent sp2 hybridization (Fig. 2.1). In a normal graphite structure, single-atom-thick graphitic layers are connected to each other by weak van der Waals force.

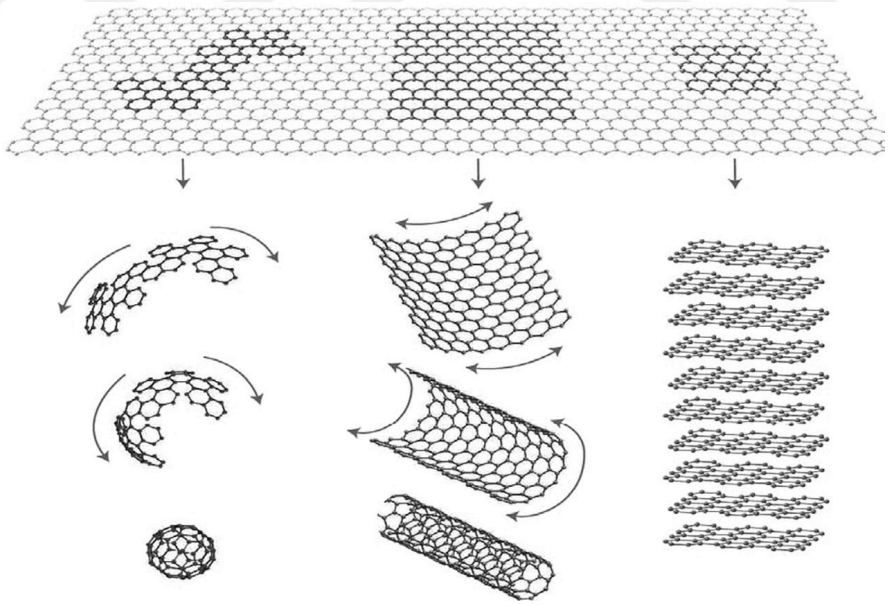


Figure 2.1 Scheme showing graphene can be wrapped up to form 0D fullerenes, wrapped up to form 1D CNTs, or stacked up to form 3D graphite (Geim & Novoselov, 2007)

The spherical form of a single layer of graphite is called 0D fullerene, and the 1D cylindrical form formed by curling from the edges is called carbon nanotube. The 2D structure consisting of one or a few layers of graphite is called graphene. When the literature information is examined, it is seen that several different methodologies are used for the classification of graphene. According to the most used classification method:

- Very few layers graphene (vFLG): one to three layers;
- Few Layers graphene (FLG): two to five layers;
- Multilayer graphene (MLG): two to ten layers;
- Graphene nanoplatelet (GNP): more than ten layers (Kauling et al., 2018)

Its classification according to the recently defined ISO standards is as follows:

- Graphene: single layer of carbon atoms;
- Bilayer graphene: two well-defined stacked graphene layers;
- Few-layer graphene: consisting of three to ten well-defined stacked graphene layers;
- Graphene nanoplatelet: thickness between 1 and 3 nm and lateral dimensions ranging from ≈ 100 nm to 100 μm.

The physical properties of graphene material vary depending on the number of layers. For example, the sheet resistance of single-layer graphene is about 2 KΩ/sq, and the optical transmittance is about 97% (X. Li, Zhu, et al., 2009). However, with increasing layer number, sheet resistance, and optical transmittance decrease. In the light of this information, when the three-layer graphene is examined, it is seen that the sheet resistance is about 700 KΩ/sq and the optical transmittance is 92%, while the sheet resistance of the four-layer graphene is 400 and KΩ/sq the optical transmittance is 89% (X. Li et al., 2009). As another example, graphene's high charge carrier density (~15,000 $cm^2/V \cdot s$) and resistivity of ~10^{-6} ohm.cm indicate that it is an ideal material to be used in field-effect transistors (Geim & Novoselov, 2007). The outstanding electrical properties of graphene are of interest for advanced technological applications

such as photovoltaic systems, biosensors, transistors, integrated circuits, conductive polymer technologies, energy storage systems.

2.1.1 Graphene Types

The final structure of the graphene product primarily depends on the number of graphitic layers that make up its structure. Theoretically, the "pristine" graphene structure should be only one atom thickness. Single layer graphene structure is only one carbon atom thick; its thickness is 0.345 nm. Although the graphene product normally consists of a single layer, structures up to 10 atomic layers of carbon thickness are called graphene in the market. Graphene is generally single-layer graphene (SLG, 1 layer of carbon), double-layers graphene (DLG, 2 layers of carbon), few-layers graphene (FLG, 3-5 layers of carbon), multi-layer graphene (MLG, 5-10 layers of carbon) and graphene nanoplatelets (graphene sheet stacks of more than 10 layers). In addition to the graphene form, which consists only of carbon layers, there are also different forms used commercially. The most popular of these different forms are graphene oxide (GO consist of carbon, oxygen, and hydrogen), reduced graphene oxide (rGO consist of less oxygen, and more carbon), powdered graphene, graphene solution, graphene paste, graphene nanoplatelets (thickness between 1 to 3 nm, lateral size between 100 nm to 100 μm), functionalized graphene (which adds elements of functional groups to the surface or edges of the graphene), and worm-like graphene, or graphite (exhibits electrical properties close to graphene) (Fig. 2.2).

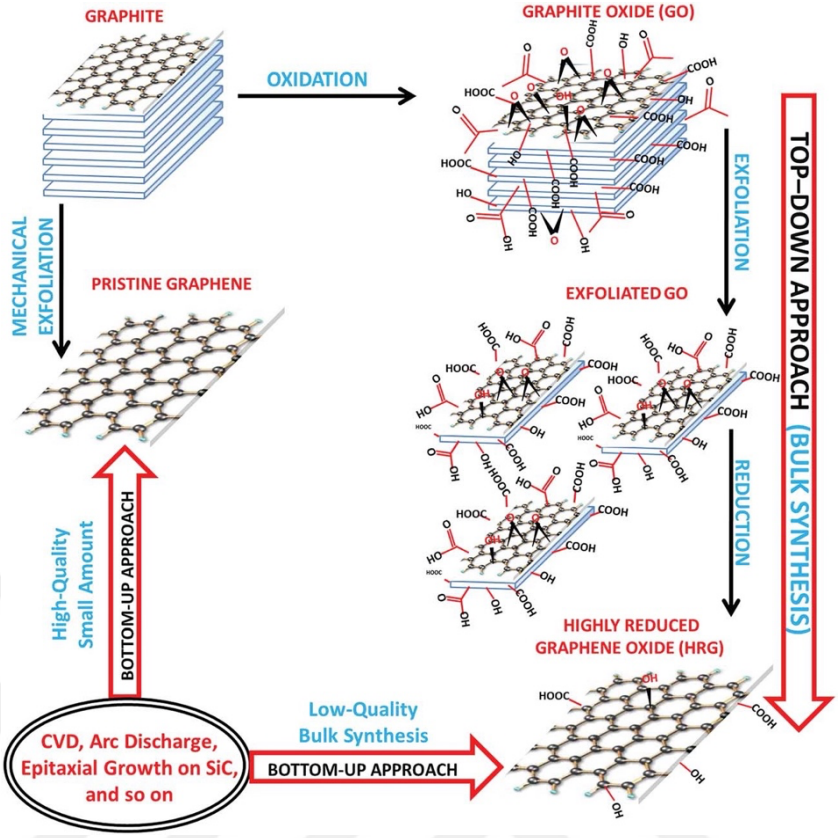


Figure 2.2 Basic graphene forms (Khan et al., 2015)

2.1.2 Graphene Production Methods

To date, many methods have been developed for the synthesis of graphene. The most important of these methods are; mechanical cleaving (exfoliation), chemical exfoliation, chemical synthesis (e.g., Hummer method and electrolysis), chemical vapor deposition (CVD), microwave synthesis, nanotube unzipping, epitaxial growth (Allen et al., 2009; Jiao et al., 2009, 2010; Kosynkin et al., 2009; Novoselov et al., 2004; Park & Ruoff, 2009; Reina et al., 2010; Viculis et al., 2003; Xin et al., 2010).

The general flow chart of graphene production methods is given in Fig. 2.3. Graphene was first produced by the chemical decomposition method in 1975. At the end of this production, the graphene structure consisting of several layers on a single crystal platinum surface was obtained. However, due to the limited characterization methods in those days, this structure could not be defined as graphene (Lang, 1975). In 1999, the cleaving of highly ordered pyrolytic graphite (HOPG) was achieved with

the help of the tips of AFM. This mechanical cleaving method has been developed to obtain graphene structure from a few layers to a single layer (X. Lu et al., 1999). Although graphene was first produced in 1975, it was first reported in 2004. Novoselov et al. used the adhesive tape to separate the graphene layers from the surface of the graphite source in their study in 2004.

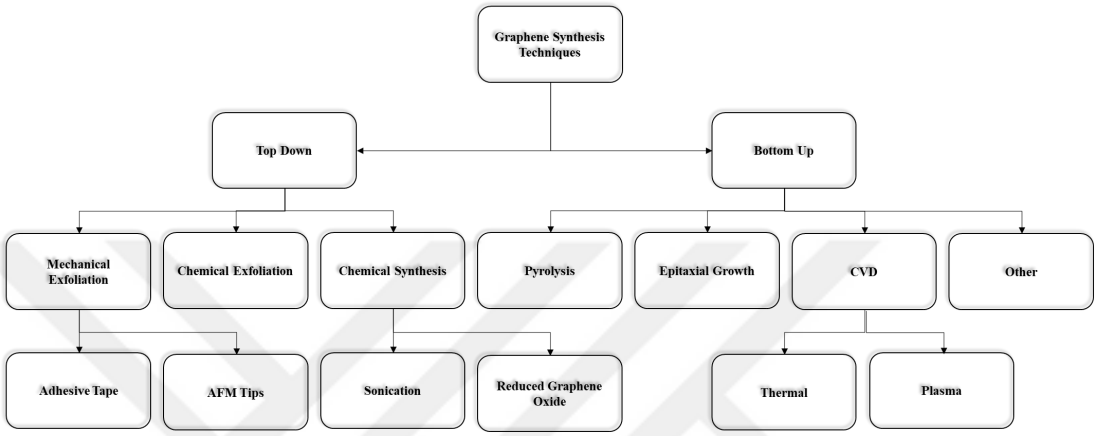


Figure 2.3 Chart of basic graphene production methods

The chemical exfoliation method is based on the principle of adding large alkali ions between the graphite layers dispersed in the solution. In this method, the weak van der Waals bonds between the graphite layers are broken by the alkali ions that have entered between the graphite layers. Another chemical synthesis method is to separate the layers of graphite after it has been oxidized. After the graphite is oxidized, the layers are separated by various mechanical effects and graphene oxide is obtained. Graphene is produced by reducing with the help of various reducing agents to obtained graphene oxide. Sometimes in chemical synthesis methods, external factors (sonic force, electric current, etc.) are used to facilitate the separation of layers.

One of the best methods in the production of graphene is the CVD method, as in the production of carbon nanotubes. In the CVD method, the separated carbon with the help of high temperature is deposited on the catalytically active transition metal. There are also different types of CVD method such as thermal and plasma enhanced.

2.1.2.1 Mechanical Exfoliation

The mechanical exfoliation method is a production method classified as top-down. The most well-known version of mechanical exfoliation is the production of graphene with the help of adhesive tape. In this method, graphene is produced by peeling the pyrolytic graphite layers, which are arranged in an orderly manner, using adhesive tape. This method is the most basic graphene production method and during this process, graphene layers are separated from graphite crystals. After peeling, multi-layers of graphene remain on the adhesive tape surface. The peeling process is done several times on top of each other to try to reduce the number of layers of graphene. The schematic representation of the method is given in Fig. 2.4. Although this method is simple to produce graphene, it is not suitable for large-scale production (Abhervé et al., 2015; Sinclair et al., 2019).

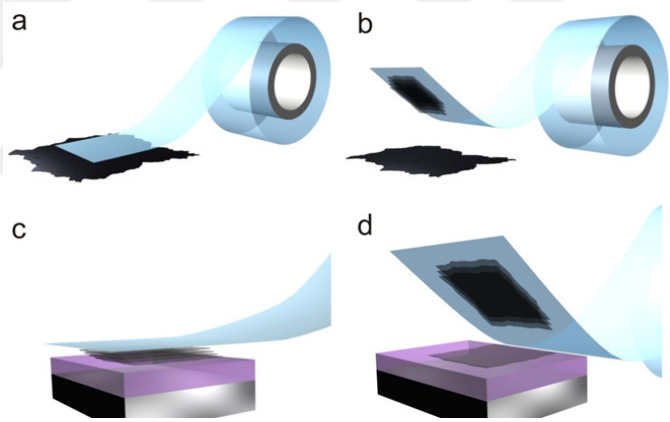


Figure 2.4 Mechanical exfoliation method (J. Li et al., 2012)

2.1.2.2 Liquid-phase Exfoliation (LPE)

Liquid phase exfoliation method is based on exfoliation of graphite with the help of ultrasonic waves in a liquid medium containing chemicals such as acetic acid, sulfuric acid, hydrogen peroxide, dimethylformamide, N-Methyl-Pyrrolidone. In the LPE method, the weak van der Waals forces between the graphite layers are broken and the graphite exfoliates. As a result of this decomposition, graphene layers are obtained. Although this method is one of the most used methods in commercial

graphene production, its biggest disadvantage is that it is very difficult to control the number of layers of the produced graphene (X. Cui et al., 2011; Monajjemi, 2017). A representative illustration of the LPE method is given in Fig. 2.5.

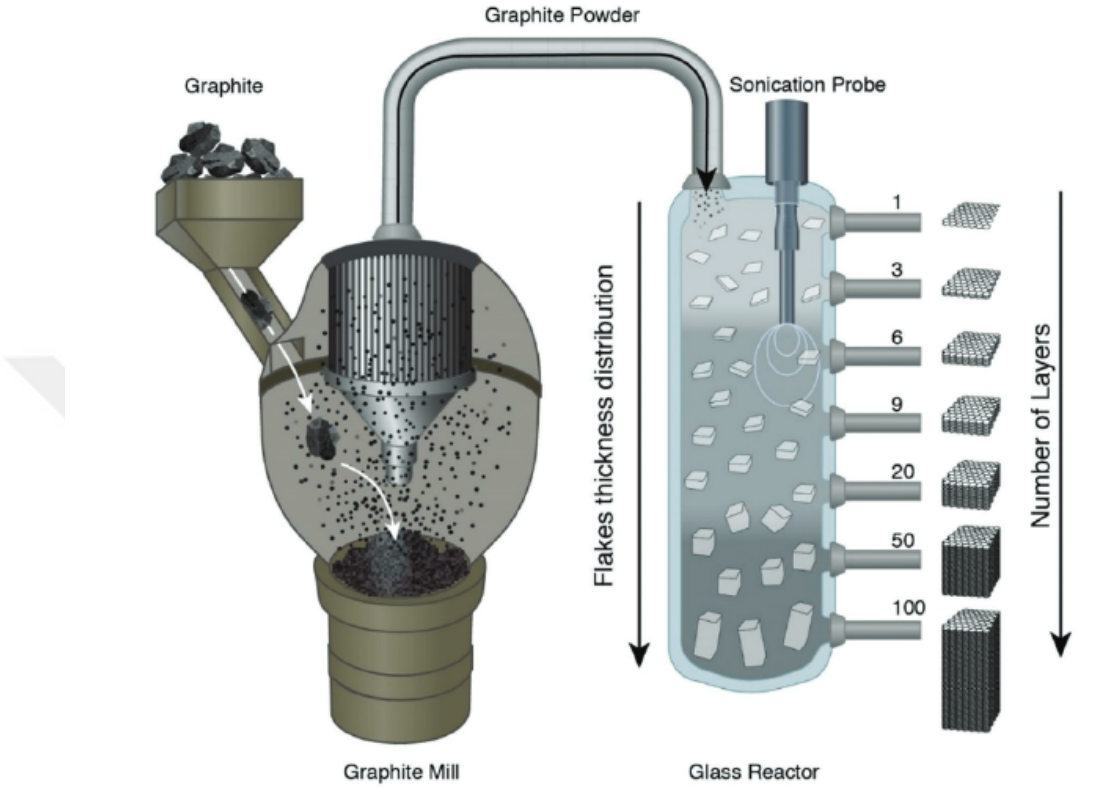


Figure 2.5 A representative illustration of the LPE method (Kauling et al., 2018)

2.1.2.3 Chemical vapor deposition (CVD)

CVD is an important deposition method used in transition metals. Nickel and copper surfaces are generally used in the production of graphene by the CVD process. The graphene film produced in the CVD process is deposited on the surface of the metallic catalyst used as the substrate. This method basically consists of two stages; a) activation of gaseous reactants and, b) Formation of stable layer as a result of chemical reaction on suitable surface. During these two stages, the carbon source (gas, solid or liquid) decomposed at high temperature accumulates on the surface of the metal catalyst in the form of a continuous film layer, forming graphene film (Muñoz & Gómez-Aleixandre, 2013; Song et al., 2012). The representative illustration of graphene production by CVD method is given in Fig. 2.6.

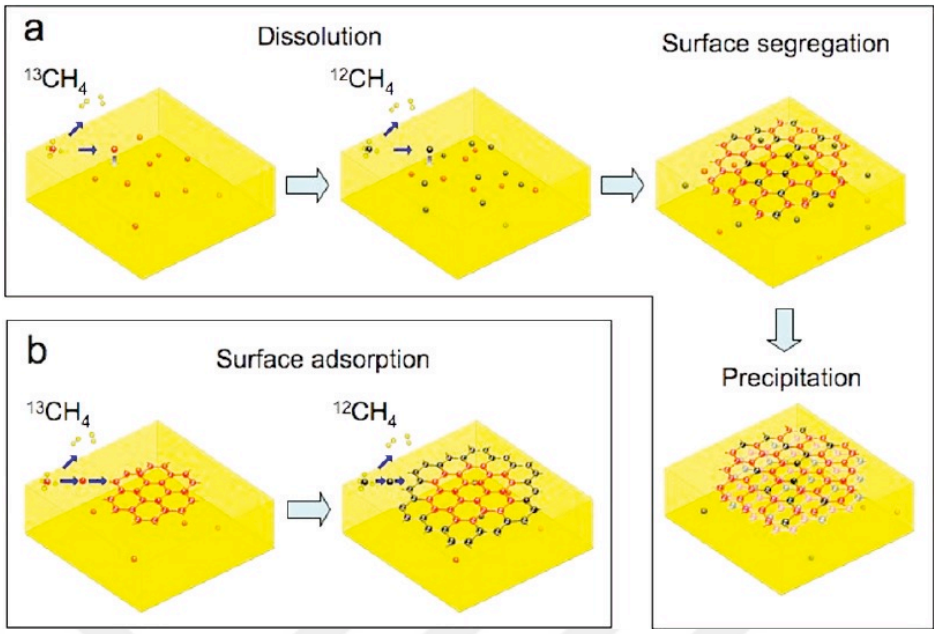


Figure 2.6 The representative illustration of graphene production by CVD method (X. Li, Cai, et al., 2009)

2.1.2.4 Reduction of Graphene Oxide

Reduction of graphene oxide is a top-down production method that enables the production of graphene by a chemical method. The first single layer reduced graphene oxide (rGO) structure, which is accepted in accordance with current literature, was obtained by Boehm et al. in 1962 (Boehm et al., 1962). In this method, the graphite is first oxidized with the help of various chemical agents ($KMnO_4$, HCl, HNO_3, H_2SO_4, etc.) and then the layers are separated from each other by external effects such as sonication or electric current. The product obtained at the end of this step is called graphene oxide (GO). Then, the GO structure obtained is reduced with the help of reducing chemical agents (N_2H_4, $C_6H_8O_7$, Vitamin-C, etc.) and the functional groups such as hydrogen and oxygen are removed from the structure. The representative illustration of explaining the basic principle of the method is given in Fig. 2.7 and the flow chart is given in Fig. 2.8. (Bosch-Navarro et al., 2012). The most well-known rGO fabrication methods using this basic principle, as shown in Fig. 2.9; Brodie method, Staudenmaier method and Hummers and Offeman method.

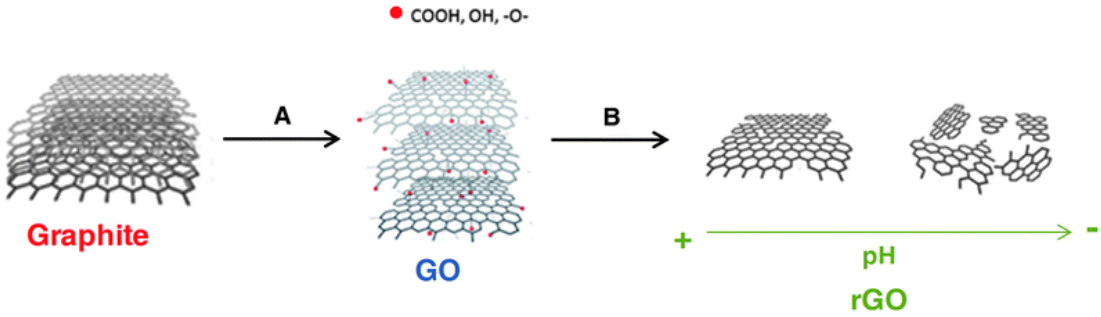


Figure 2.7 The representative illustration that explains the basic principle of the reduction of graphene oxide method (Bosch-Navarro et al., 2012)

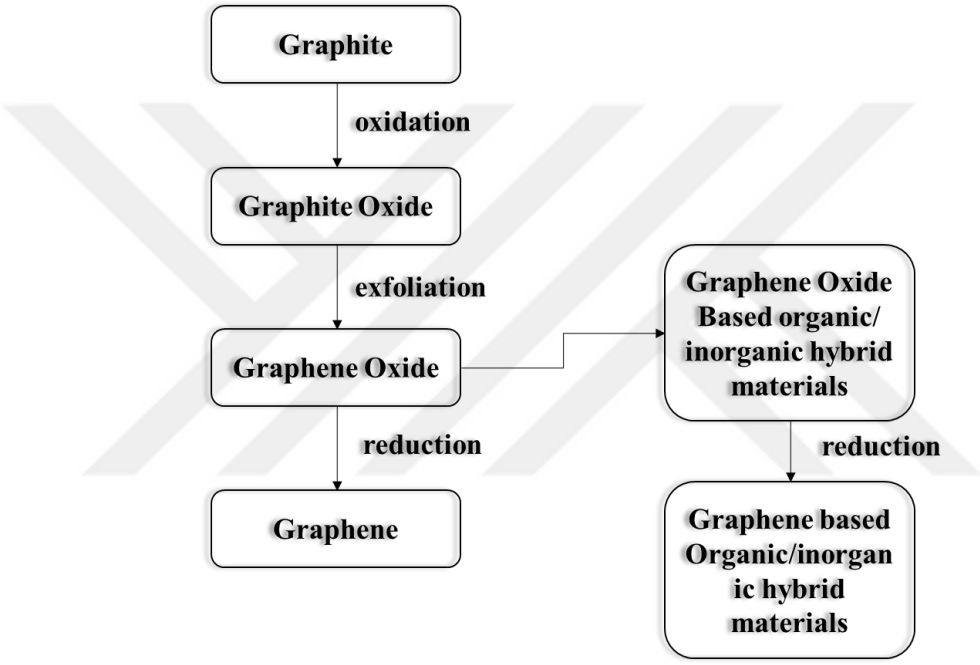


Figure 2.8 Reduced graphene oxide production flowchart

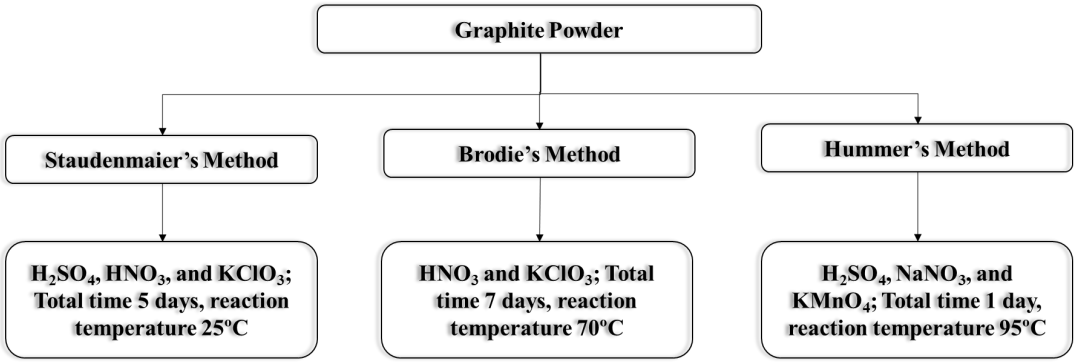


Figure 2.9 The most well-known rGO fabrication methods

2.1.3 Application of Graphene

Graphene is being studied for use in many advanced technological applications, thanks to its extraordinary properties such as high electrical and thermal conductivity, high optical transmittance, excellent mechanical strength, and large surface area. The most important areas where graphene-containing products will emerge in the near future are; battery technologies, transistors, computer chips, power generation technologies, supercapacitors, water filters, antennas, touch screens, photovoltaic systems, flexible electronics, etc.

2.1.3.1 Energy

Today, one of the most important issues related to graphene is the use of graphene in renewable energy production. Thanks to the superior properties of graphene, different types of solar cells can be produced to convert solar energy into different types of energy (Redondo-Obispo et al., 2020). For example, graphene-based solar cells are used in applications such as solar-thermal or solar-electricity conversion (Díez-Pascual et al., 2018). Thanks to its 2D graphene structure, excellent electrical and thermal conductivity, high transparency, flexibility, outstanding mechanical strength, and large specific surface area, it is a promising material in energy applications. The most important reason for its success in this field is that it can exhibit high electrical conductivity without affecting optical transmittance in solar cell applications (Munuera et al., 2016). In addition, thanks to graphene/polymer composite structures, dye-synthesized solar cells (DSSC) are produced and solar energy is converted into electrical energy. It has been observed that graphene-based conductive polymer composites are used in supercapacitors or ultra-supercapacitors and outperform conventional batteries (J. Ma et al., 2017; Pan et al., 2016). Graphene films (<100 nm) produced by various methods can be coated on flexible surfaces such as PET. In this way, it is possible to use the produced supercapacitors in flexible and wearable energy storage systems (Chen et al., 2018; Gao, 2017). As another application, graphene filling can significantly change the electrical conductivity potentials of insulating polymers. With this method, electrically conductive flexible

polymeric structures can be formed (AbdelHamid et al., 2016). For example, GO and rGO-doped Polyaniline (PANI) polymer is an important material used to manufacture high-performance capacitors (R. Wang et al., 2017; Q. Wu et al., 2010). In Fig. 2.10, the illustration representing the graphene-based energy conversion and storage systems is given (Z. Wang & Liu, 2015).

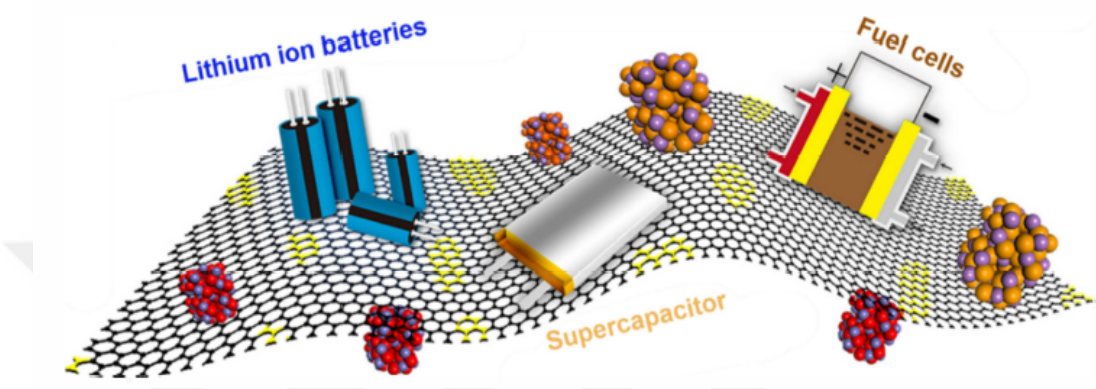


Figure 2.10 The illustration representing the graphene-based energy conversion and storage systems (Z. Wang & Liu, 2015)

Another energy storage system in which graphene is used is lithium-ion batteries (LIBs). One of the biggest problems in lithium-ion batteries is the continuous expansion and contraction of the volume as a result of the lithiation/de-lithiation reaction between the anode and the cathode (H. J. Kim et al., 2020; Pender et al., 2020). However, another problem is that the existing electrodes used in lithium-ion batteries cannot provide sufficient electron conductivity. Graphene's high electron conductivity and highly porous structures have been utilized to overcome these problems (J. bin Wu et al., 2018; C. Xu et al., 2013).

2.1.3.2 Wearable Technologies

The main purpose in graphene-based wearable technologies is to create a structure that combines flexible fiber-based supercapacitors with excellent electrochemical properties. There are different approaches to design supercapacitors that can use energy storage and wearable technologies. Especially among these applications,

supercapacitors with high flexibility, excellent cycle number and mechanical stability are remarkable. rGO/transition metal oxide hybrid fiber structures have been used for such applications. For example, in this application, the electrochemical performance of the fibers increased significantly as a result of the synergistic effect between the rGO and the metal oxide (J. Ma et al., 2017). In another study, it was observed that the electron transport ability of symmetrical supercapacitors improved thanks to the conductive graphene network, and it maintained its electrochemical stability even under harsh conditions such as bending and bending (Jin et al., 2018). In another study, it was observed that supercapacitors produced using graphene and MnO2 retain their capacity up to 93% after 1000 cycles (Lim et al., 2017). Another important application area where graphene is used is gas sensors. The most important parameters for gas sensor materials are selectivity, sensitivity, response time, detection limit, etc. Graphene doped fabric knits can be produced in meter scale with excellent electrothermal conversion efficiency, high sensitivity, fast response (<0.5 s), resistance to organic solvent vapor (~5000 cycles) (G. Cui et al., 2020). Apart from these, graphene-based sensors used as wearable devices are also used for the determination of body temperature, blood pressure and heart rate control in humans (Iqbal et al., 2020). Brief illustration of the graphene-based sensor platform for health monitoring is given in Fig. 2.11.

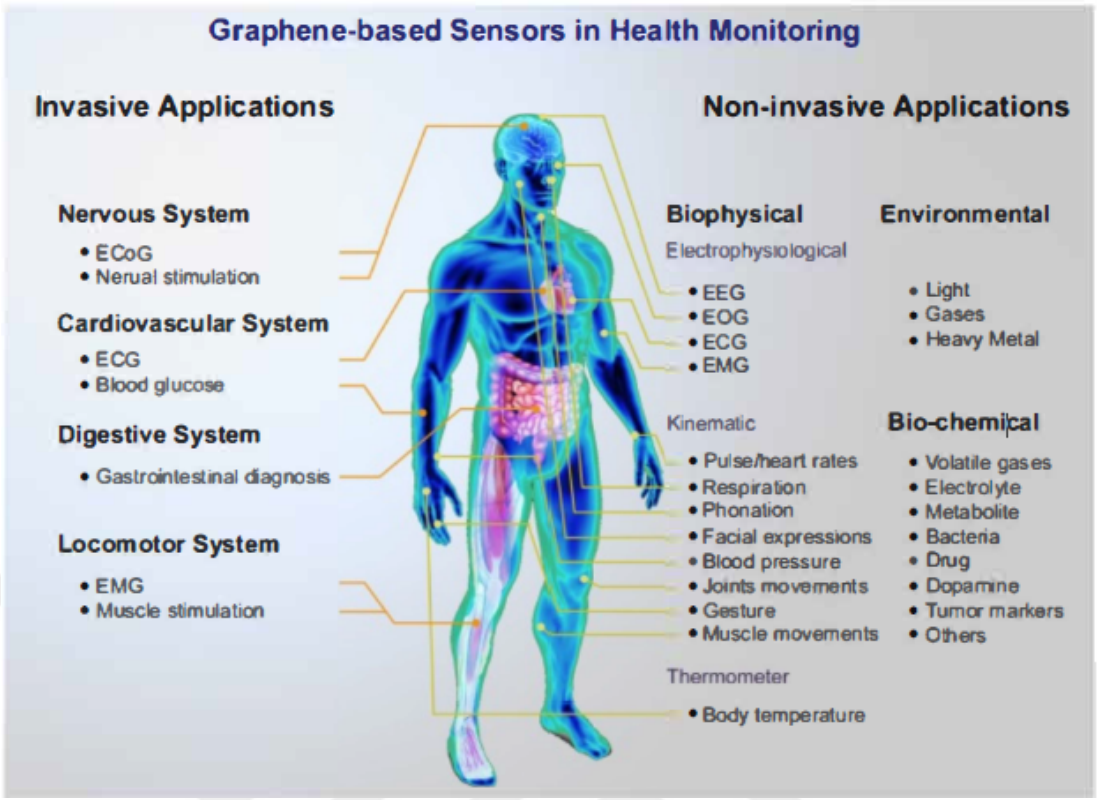


Figure 2.11 Brief illustration of the graphene-based sensor platform for health monitoring (Huang et al., 2019)

2.1.3.3 Wastewater Management

Water pollution is increasing day by day due to various toxic organic and inorganic wastes released from sources such as industrial and household applications and agricultural applications. This situation poses a great threat to aquatic creatures. In addition, access to clean water resources, which are necessary for people to continue their vital activities, is also getting harder. For such reasons, the porous structure of graphene is used to clean wastewater. Graphene-containing nanomembranes act as an important barrier against toxic materials in the purification of both liquid and gaseous materials (Arheimer, 2016; Y. Wang et al., 2020). A schematic representation of graphene-based membranes is given in Fig. 2.12.

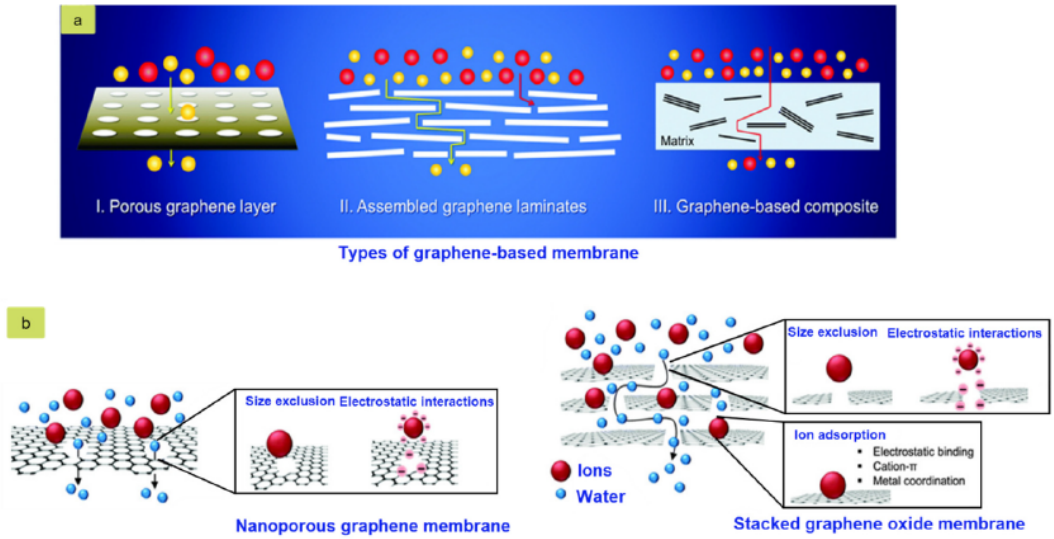


Figure 2.12 (a) Different types of graphene-based membranes, (b) Water separation membrane (Iqbal et al., 2020)

2.1.3.4 Medical Applications

Properties such as large surface area, hydrophobic structure and chemical stability of graphene have shown positive results for biomedical applications. These features have made it possible to conduct studies on subjects such as drug delivery, gene therapy, DNA sequencing, cancer treatments, and bioimaging (Z. Liu et al., 2008; X. Sun et al., 2008). The developed graphene-containing fibers have demonstrated antimicrobial properties against gram-positive and gram-negative bacteria. These properties of fibers hold significant potential for tissue engineering, biotechnical and biomedical applications (X. Hu et al., 2017). Thanks to special polymer structures containing graphene, biomolecular structures such as glucose, hemoglobin, cholesterol, and DNA can be determined precisely (Bobrinetskiy & Knezevic, 2018; Y. Wang et al., 2011). Although graphene provides extraordinary opportunities for medical applications, it is not yet known what its long-term effects on the human body will be. Applications of graphene-based materials in medical are given in Fig. 2.13.

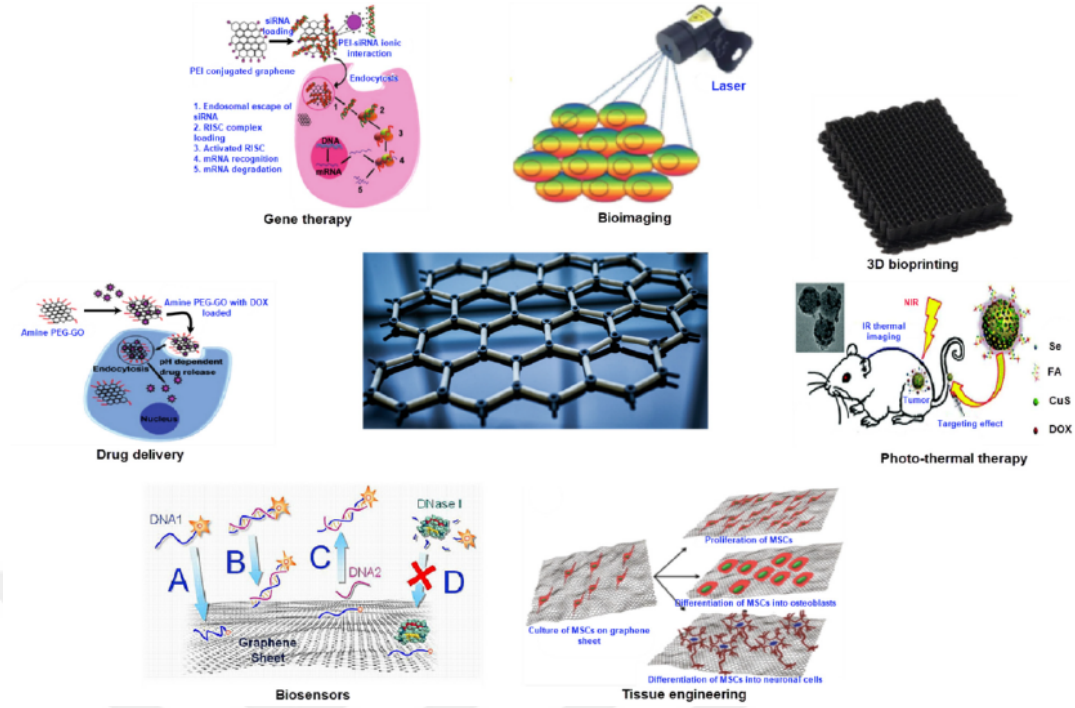


Figure 2.13 Applications of graphene-based materials in medical (Syama & Mohanan, 2019)

2.1.3.5 Composite Industry

Automotive, aerospace and marine sectors are among the sectors where composite products are used the most (al Faruque et al., 2021; Anand et al., 2021; Cai et al., 2021; Yadav et al., 2020). Especially in these sectors, it is very important to lighten the weight of the part and reduce fuel consumption. The mechanical properties of graphene/carbon fiber/polymer composites such as interlayer shear strength and fracture toughness showed very good results. Thanks to the superior mechanical properties obtained, it is used in very important parts such as air-craft ribs, fuel tanks, tail assemblies, body panels, wing parts (Kumar et al., 2019; Othman et al., 2019). In addition to these applications, EMI materials, which have an important place in the aerospace industry, are also being developed thanks to epoxy composites containing graphene. Another important feature for material technologies is corrosion resistance. It is a product of commercial value today in graphene-added dyestuffs developed to increase the corrosion resistance of materials (G. Cui et al., 2019). Another application area that can be given as an example of graphene/polymer composites is flame retardant materials. The developed flame retardant materials can be used in important

areas such as battery packs, electronic devices, hospital applications, and fireproof textile products (Sang et al., 2016).

2.2 Battery Systems

Batteries are electrochemical systems that produce electrical energy as a result of redox reactions. Batteries consist of two electrodes, anode and cathode. These electrodes are produced from materials such as metals, carbon-based conductive materials, semiconductors and conductive polymers. Between the anode and the cathode is the electrolyte, an ionic conductor that prevents the electrodes from coming into direct contact with each other. If the contact of the electrodes is not prevented, the battery will short-circuit, resulting in situations such as burning and explosion. The illustration summarizing the basic battery system is given in Fig. 2.14.

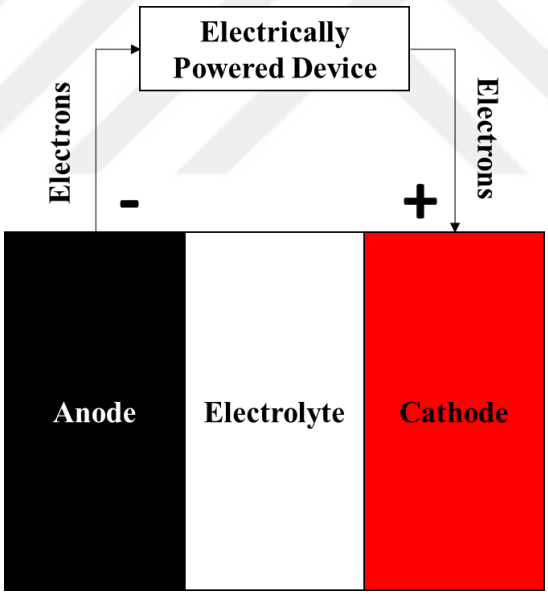


Figure 2.14 The basic battery system

2.2.1 Battery Types

Batteries are generally divided into three classes. Primary batteries are disposable batteries and cannot be charged repeatedly. Secondary batteries are rechargeable batteries and can be restored to their original state after charging. Another battery class

is batteries produced for special applications that are not used for general purposes. Apart from this main classification, there are also batteries used for military and medical purposes, which do not have a wide commercial network due to cost and limited market. The schematic representation and applications of representative rechargeable batteries are given in Fig. 2.15.

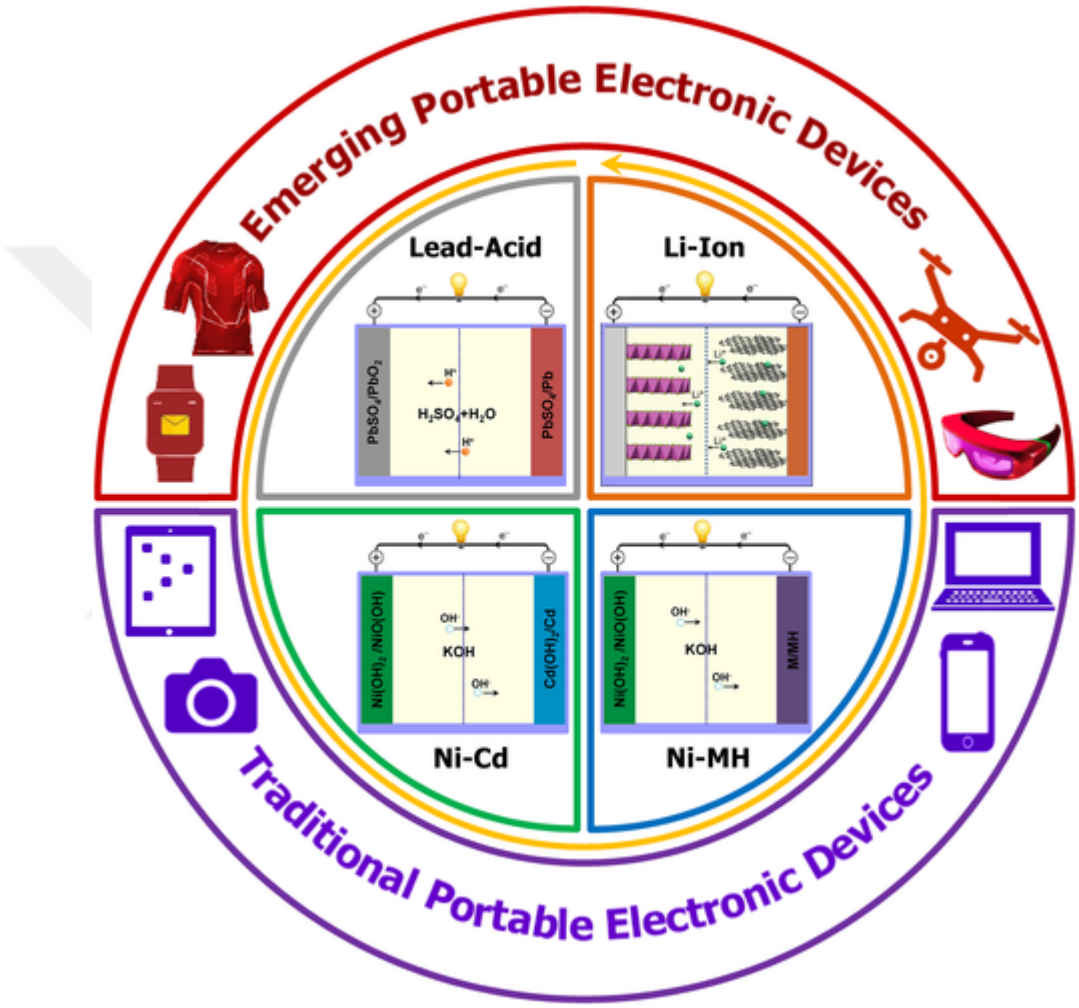


Figure 2.15 Schematic illustration of representative rechargeable batteries and their applications (Liang et al., 2019)

Lead-acid battery is a rechargeable battery, invented by the French physicist Gaston Planté in 1859. In addition, this battery is the owner of the title of the first rechargeable battery. Basically, the lead-acid battery cell consists of a lead anode and a lead-oxide cathode. Between the anode and the cathode, there is sulfuric acid, which acts as an electrolyte. The anode and cathode in the battery cell react with acid to produce lead

sulfate. While these reactions take place, the anode releases electrons while the cathode consumes electrons. Lead-acid batteries have a relatively low energy density compared to other batteries. Despite this, it is capable of supplying high pulse currents. Thanks to this feature, it is a type of battery used to provide the high current needed by the starter motors. Another advantage of lead acid batteries is their low internal resistance. Thanks to this feature, it can be used to supply power to more than one circuit. Lead acid batteries are currently used in applications where weight can be tolerated, such as automobiles (May et al., 2018; Rand & Moseley, 2009; Schmidt-Rohr, 2018).

Nickel-cadmium (NiCd) battery was invented ed by Swedish chemist Waldemar Jungner in 1899. This battery is a type of rechargeable battery with nickel and cadmium electrodes in an alkaline (potassium hydroxide) electrolyte. Nickel-cadmium batteries convert chemical energy into electrical energy during discharge, and electrical energy into chemical energy during charging. Nickel-cadmium batteries are approximately 30 times more durable than lead-acid batteries in terms of charge/discharge cycles. Although there are various types of these batteries, the most used types are ventilated and sealed. It is preferred in many applications thanks to its features such as long battery life, high energy density, wide temperature range (Hariprakash et al., 2009; Liang et al., 2019).

Nickel metal hydride (NiMH) batteries are a type of rechargeable battery, just like nickel-cadmium batteries. In these batteries, instead of the cadmium electrode in nickel-cadmium batteries, an alloy capable of absorbing hydrogen is used. Nickel oxyhydroxide (NiOOH) is used as the positive electrode. NiMH batteries can store 3 times more energy than NiCd batteries. Due to its high capacity, the operating time of the battery increases without additional volume and weight gain. The most important disadvantage compared to NiCd batteries is that they are highly affected by temperature changes (Ayeb et al., 2006; Hariprakash et al., 2009).

Lithium-ion battery (LIB) systems were first introduced by British chemist M. Stanley Whittingham. LIBs are the most common secondary battery system used in portable electronic devices. Thanks to its low density, high electrochemical potential,

and high energy-to-weight ratio, lithium metal is considered the most ideal material to be used in battery production. LIBs generally consist of a graphite anode and a lithium-containing cathode ($LiCoO_2$, $LiFePO_4$, $LiMn_2O_4$, $LiNiCoMnO_2$, etc.). Between these two electrodes, there is an electrolyte liquid that allows the passage of lithium ions. Compared to traditional batteries such as NiCd, NiMH, it has become the highest performance secondary battery chemistry due to its higher energy density, high operating voltage, low maintenance requirements (Nitta et al., 2015).

2.2.1.1 Lithium-Ion Battery

Since lithium-ion batteries can offer high energy and high-power density together, they have become a frequently preferred technology for electrical appliances and electric vehicles (Tarascon, 2010). Greenhouse gas emissions will be significantly reduced when fossil fuel-powered vehicles are replaced by fully electric vehicles (Pacala & Socolow, 2004). The high energy efficiency of lithium-ion batteries will allow to improve the quality of electrical energy produced from solar, wind and other renewable energy sources. For this reason, lithium-ion batteries are of great interest to both industry and governments, and numerous studies are being conducted on them. Although there are many studies on lithium-ion batteries today, there are some who think that lithium-ion batteries cannot fully meet the energy storage needs in the future. The biggest concern in this regard is the resource shortage in the supply of Li and some of the transition metals used in lithium-ion batteries (Vikström et al., 2013). Despite all these disadvantages, lithium-ion battery chemistry has significant advantages compared to other battery chemistries. The fact that lithium is the metal with the lowest reduction potential ensures that lithium-ion batteries have the highest cell potential. Also, thanks to lithium being the third lightest metal and having a very small ionic radius, Lithium-ion batteries can have high gravimetric and volumetric capacity and power density (Nitta et al., 2015). The amount of ionic diffusion in battery electrodes is one of the most important parameters affecting battery power. This is the biggest obstacle to developing alternative battery chemistry. Researchers think that the lithium raw material problem will not occur in the near future (Gruber et al., 2011). In the past, it has been said that there will be resource scarcity for oil, but with the developing

technology, oil resources and reserves have been increased. It is stated that the amount of known lithium source is sufficient to meet the needs of the global automobile market (Grosjean et al., 2012; Speirs et al., 2014). When the situation is analyzed in terms of cost, Li constitutes a very small part of the total cost. The largest cost in the manufacture of lithium-ion batteries belongs to the cathode material cobalt and the process (Nitta et al., 2015). Considering all these situations, it is likely that lithium-ion batteries will continue to be widely used in energy storage for many years. Since lithium-ion batteries are the most commonly used among portable batteries, it is very important to reduce costs and increase their performance, expand the field of application, and reveal new technologies. The energy and power densities of batteries can be improved thanks to electrodes with higher rate capacity, higher energy storage capacity, and higher voltage. Thanks to these improvements, smaller and cheaper lithium-ion batteries will be produced. In Fig. 2.16(a), the number of various metals in the world and their average sales prices are given (Nelson et al., 2019).

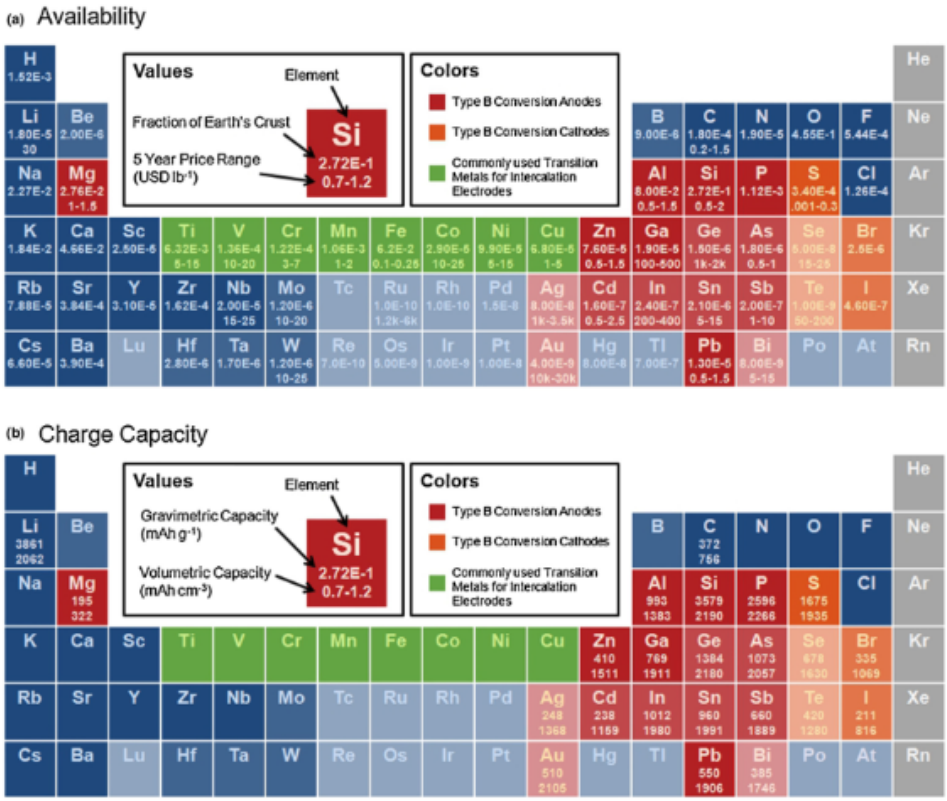


Figure 2.16 The number of various metals in the world (a) and their average sales prices (b) (Nelson et al., 2019)

The quantities of elements represent the limit on the availability of the element. In Fig. 2.17(c), the theoretical and specific volumetric capacities of the elements entering the conversion reaction with lithium are given. However, most of the materials used as cathodes are in the form of compounds (Fig. 2.17(b)).

Therefore, in Fig. 2.17(d), a graph describing the average electrode potential versus the experimentally achievable (for anodes and intercalation cathodes) or theoretical (for conversion cathodes) capacity is given. Also, the table in Fig. 2.17(a) can be used to determine the electrolyte material (Gwon et al., 2014; Y. Hu & Sun, 2014; Tarascon, 2010; X. Wang et al., 2014; Xie & Wei, 2014; Zhou et al., 2014).

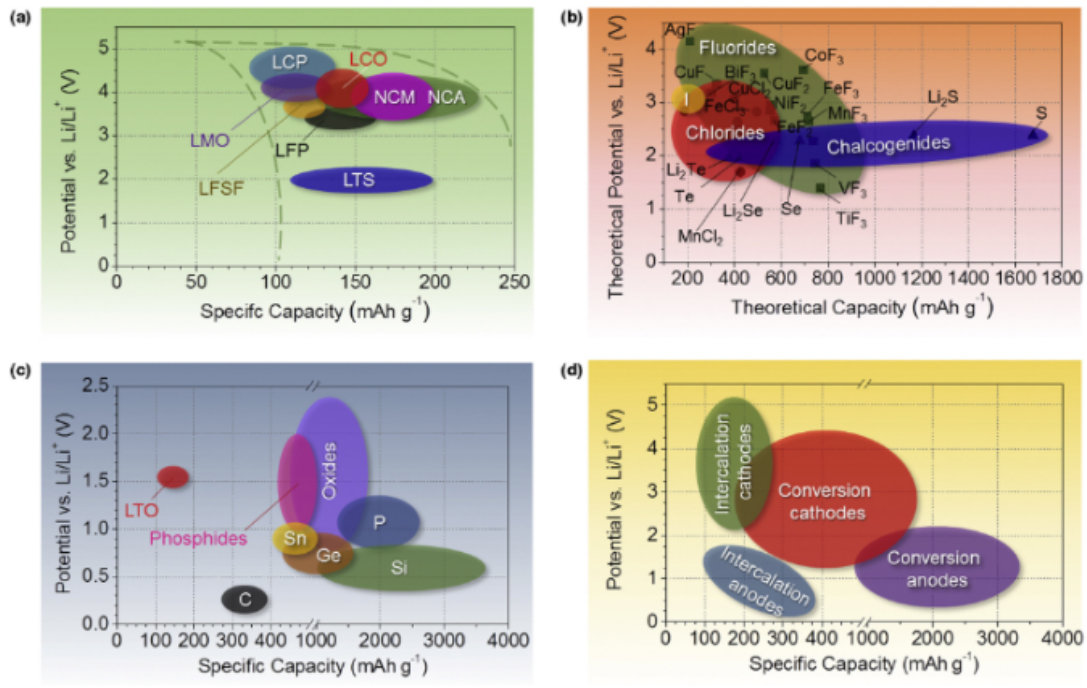


Figure 2.17 The theoretical and experimental values of electrical potential and capacity of varios materials used in Li-ion battery system (LCO: lithium cobalt oxide, LMO: lithium manganese oxide, NCM: nickel cobalt manganese oxide, NCA: nickel cobalt aluminum oxide, LCP: lithium cobalt phosphate, LFP: lithium iron phosphate, LFSF: lithium iron fluorosilicate, LTS: lithium titanium sulfide)

Lithium-ion batteries basically consist of cathode, anode, electrolyte and separator. In the charging state, as shown in Fig. 2.18, lithium ions in the cathode electrode pass

from the electrolyte to the anode material through a separator. In the discharge state, the flow occurring in the charging state is reversed.

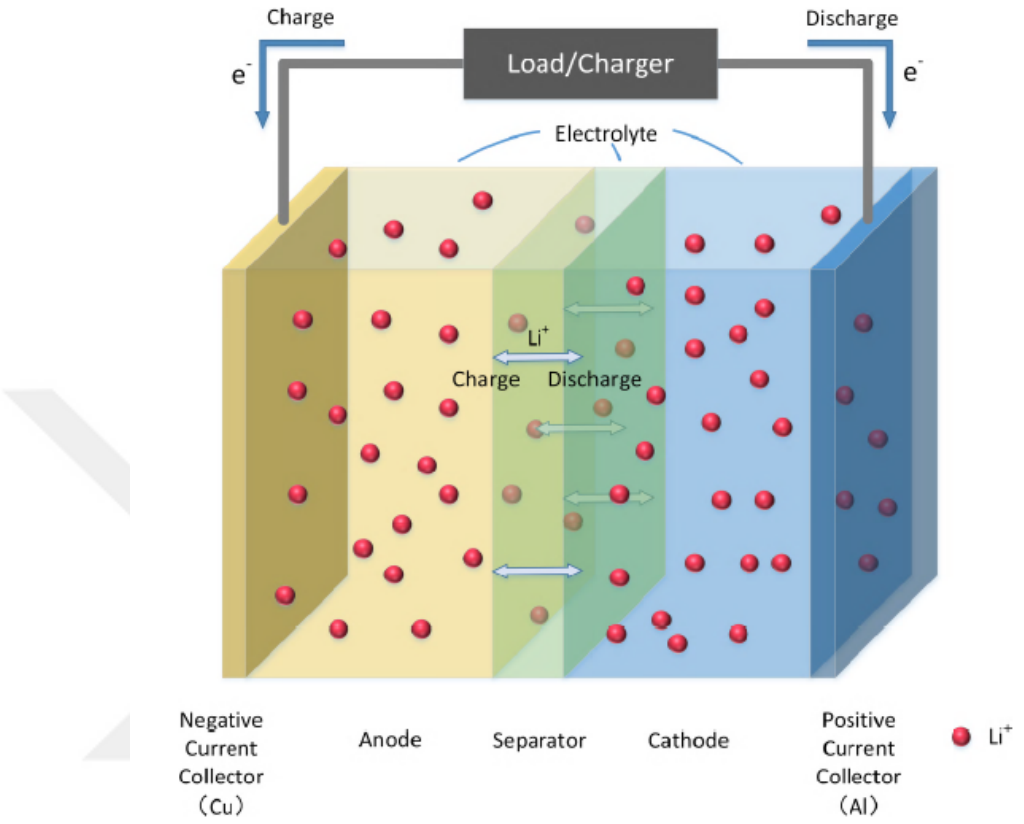


Figure 2.18 Lithium-ion battery working principle (J. Zhang et al., 2018)

A properly designed lithium-ion battery cell must have certain key features. Firstly, in order to maximize the energy density, the cathode and anode materials must allow high levels of lithium ions to move (in and out of the electrode). Secondly, the cathode material should have the lowest chemical potential and the anode material the highest chemical potential for maximizing the cell voltage and accordingly the energy density. Thirdly, the voltage variations in the cathode and anode material should be minimal during the charging and discharging processes. In addition, the diffusion coefficient of lithium should be high for high charge and discharge performance. In Fig. 2.19, the operating voltages of the compounds that give reversible reactions with lithium due to metallic lithium are shown. As can be seen from the figure, $LiCoO_2$, $LiMn_2O_4$, and $LiFePO_4$ compounds have the highest electrode potential in the 3.5 V - 4 V range. For

this reason, in today's electrode materials studies, especially these 3 compounds are emphasized (Delmas et al., 1993; Gummow & Thackeray, 1992; Rossen et al., 1992).

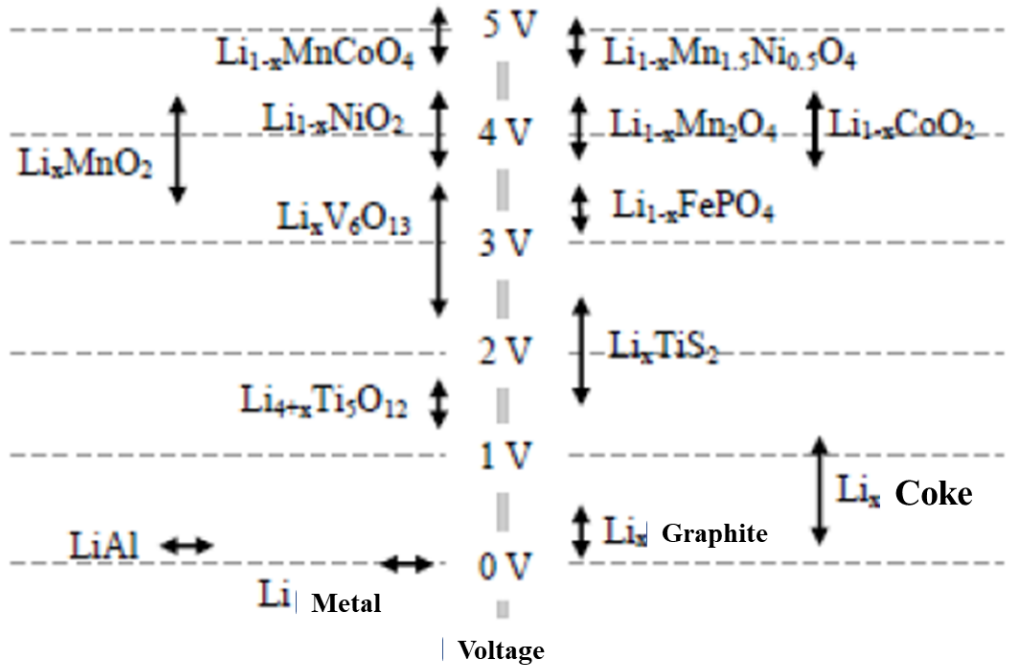


Figure 2.19 Electrochemical potentials of compounds that give reversible reactions with lithium due to metallic lithium (Delmas et al., 1993; Gummow & Thackeray, 1992; Rossen et al., 1992)

When the most common batteries used commercially today are examined, it is seen that they contain graphite-based anode and $LiCoO_2$ cathode. The commercial profit of $LiCoO_2$ used as the cathode material is low, the Li1-xCoO_2 structure formed as a result of the separation of lithium from the $LiCoO_2$ structure (while $x > 0.5$) limits the applied voltage range to below 4.2V. In addition, the fact that its capacity in practical applications (140 mAh/g) is considerably lower than its theoretical capacity (273 mAh/g) is the main disadvantage in the use of this cathode. Considering the relatively high cost of cobalt, the search for a new generation cathode material has begun for electric vehicles in which large-diameter electrodes will be used (Amatucci & Tarascon, 2002; Thackeray et al., 1983). $LiMn_2O_4$ cathodes were first introduced by Thackeray et al. This electrode has become an important alternative cathode material with its low toxicity and cost. The operating voltage of this cathode is about 4.0V and its thermal stability is much better than $LiCoO_2$ structure. The disadvantage of this cathode is its low specific capacity (120 mAh/g) and the capacity losses that occur

when it dissolves into the electrolyte as Mn3+ ion during the cycle. Compared to two-dimensional layered materials, $LiMn_2O_4$ has a three-dimensional structure. Although it has a three-dimensional structure, the $LiMn_2O_4$ structure resembles layered structures. This similarity led to the development of laminated-spinel composite cathodes. These composite cathodes are obtained by mixing $LiMn_2O_4$ or $Li_{1+x}Mn_{2-x}O_4$ and different layered cathodes. With this composite structure obtained, cathodes with high thermal stability and cycle life were produced (Johnson et al., 2004; Thackeray et al., 2005). The most striking development among the cathode materials is the use of $LiFePO_4$ cathodes. The operating voltage of $LiFePO_4$ cathodes is 3.4V and the capacitance values obtained are close to their theoretical capacity of about 170 mAh/g. In addition, these cathodes can maintain their stability significantly after hundreds of cycles (Arnold et al., 2003; Chung et al., 2002; Herle et al., 2004; Kwon et al., 2004; Padhi et al., 1997; Ravet et al., 2001; Yamada et al., 2001). The structures of $LiCoO_2$ with a layered structure, $LiMn_2O_4$ with a spinel structure and $LiMn_2O_4$ with an olivine structure are shown in Fig. 2.20.

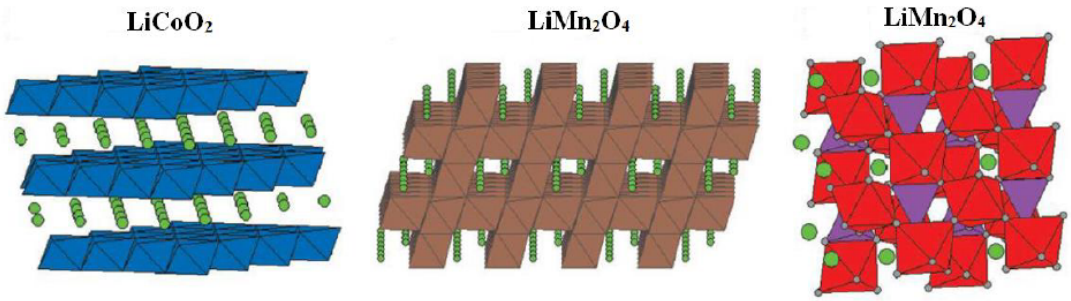


Figure 2.20 The structures of $LiCoO_2$ with a layered structure, $LiMn_2O_4$ with a spinel structure and $LiMn_2O_4$ with an olivine structure (Arnold et al., 2003)

Lithium-ion batteries use non-aqueous solvents that can dissolve enough lithium salt with sufficient polarity. Electrolytes used in lithium-ion batteries are: liquid electrolytes, polymer gel electrolytes, polymer electrolytes, ionic liquids, ceramic electrolytes. Liquid electrolytes are solutions prepared by dissolving lithium salts in polar organic solvents. Electrolytes are generally prepared from materials containing linear carbonates, esters, ethers and different salts such as lithium perchlorate $LiClO_4$, hexafluoro arsenate $LiAsF_6$, lithium tetrafluoroborate $LiBF_4$. In many studies,

electrolytes in which the $LiPF_6$ salt is dissolved with ethylene carbonate (EC) and one more carbon-containing solvent, usually dimethyl carbonate (DMC) or diethyl carbonate (DEC), are preferred (K. Xu, 2004). Polymer-gel electrolytes are the gelled form of commercial liquid electrolytes. The generally used polymer gel electrolyte is poly(vinylidene-fluoride-cohexafluoropropylene) PVDF-HFP and $LiPF_6$ dissolved in an organic solvent. Ionic liquids are a promising new class of electrolyte materials. They can remain liquids over a wide temperature range, have low volatility, high decomposition temperatures, very low ignition characteristics, and are stable over a wide voltage range (Shukla & Prem Kumar, 2008). Inorganic ceramic electrolytes are used in thin-film solid-state batteries. This lithium-ion battery system was developed for circuit boards and semiconductors. Thin-film solid-state batteries are used as a power source on chips or circuits in microelectronic devices. They can be produced by being resistant to high temperatures and by deposition techniques on silicon wafers. Conductive lithium materials such as lithium phosphorus oxynitride (LiPON) can be used as electrolytes in these cells (Neudecker et al., 1999).

2.2.2 Anode Materials

The most important criteria in the selection of anode material are to provide a sufficiently large cell voltage and to have a lower reduction potential for lithium than for the cathode. Another important feature for the anode material is that it does not lose its electrical conductivity by maintaining its structural stability after charge-discharge cycles (Shukla & Prem Kumar, 2008). Today, the most preferred anode materials are carbon-based materials. Graphite and graphitic materials are generally used as carbon-based materials. The features of carbon materials such as relatively low cost, reversibility for lithium insertion, and working in harmony with many electrolytes make it very attractive (Nitta et al., 2015). One of the most preferred anode materials in recent years is carbon and lithium alloy metals. The host element in the graphite intercalation compound protects the added lithium, reducing the possibility of reaction with the electrolyte. In addition, the charge-discharge performance of this type of anode material also depends on the diffusion rate of the lithium in the host matrix. Metals that can store lithium as an alternative to carbon materials are among

the interesting anode materials. Aluminum, tin, silicon etc. metals and semiconductor states can provide much higher battery capacity compared to graphite (Y. Liu et al., 2019). In addition, these materials contain many atoms per formula unit. However, the capacity to store so much lithium brings with it some disadvantages. The main disadvantage here is the extraordinary volume increase during the storage of large quantities of lithium. This continuous volume increase-decrease cycle causes the electrode to crack, rupture, or significantly reduce its charge storage capacity (Zhang et al., 2011).

2.2.2.1 Graphene Anode Materials

A single carbon atom thick 2D graphene structure has been found to have many outstanding physical, chemical and mechanical properties. Thanks to the high-quality sp2 hybridized carbon structure in the graphene structure, it has been observed that the electrons move ballistically even at ambient temperature (Miao et al., 2007; Novoselov et al., 2004; Paek et al., 2009; Peres et al., 2006). Graphene can be used as the anode material that allows reversible reactions in lithium-ion batteries. The reason why carbon materials are used so intensely in anode production is that they can stack a large amount of lithium between carbon layers during the intercalation process. The main reasons for the use of graphene as an efficient anode material are as follows: its ability to embed lithium in the cavities in its structure, the ability of lithium to be stored on both sides of the carbon sheet, the covalent bonding of lithium, and the ability of lithium to bind to the hydrogen-terminated ends of graphene (P. Guo et al., 2009b; G. Wang, Shen, et al., 2009; G. Wang, Wang, et al., 2009).

Graphene's large surface area and very high electrical conductivity make it a suitable material that can be used to store lithium in reversible reactions in lithium-ion batteries. The 2D structure of graphene allows lithium to be arrayed on both surfaces. In this way, graphene can create a battery capacity of 744 mAh/g (formation of Li_2C_6) according to theoretical calculations. Graphene's large surface-area-to-volume ratio and nano-void structure make it have very good lithium storage capacity and very good cyclic performance. Therefore, graphene is expected to replace graphite (372 mAh/g)

in the near future (Doh et al., 2011; Stankovich et al., 2006). The various structural properties of graphene are given below:

- Having a wrinkly structure by nature
- Graphene layers have a graphitic crystal structure
- It has a very large surface (≈ 800-1000 m^2/g) area compared to graphite.

It is possible to use different methods for the production of graphene. Graphene sheets can be obtained by first oxidizing graphite to produce graphene oxide, followed by chemical or thermal reduction (P. Guo et al., 2009a; Lian et al., 2010a; G. Wang, Shen, et al., 2009; G. Wang, Wang, et al., 2009). Another way to produce large quantities of graphene is to expand the graphite at very high temperatures (about 1000 degrees Celsius) in a short time (X. Li, Wang, et al., 2008; McAllister et al., 2007). Another method is to obtain graphene by decomposition of graphite directly by mechanical or electrochemical means (J. Lu et al., 2009; Novoselov et al., 2004). As an alternative to these methods, production methods such as bottom-up CVD, epitaxial growth, and solvothermal method can be used (Berger et al., 2006; Coraux et al., 2008; Dato et al., 2008; K. S. Kim et al., 2009; Reina et al., 2009; Sutter et al., 2008). Although the properties of graphene vary according to the method of preparation, they provide higher anodic capacity than graphite as the anode material for lithium-ion batteries (Hernandez et al., 2008; X. Li, Zhang, et al., 2008; Lian et al., 2010b).

CHAPTER THREE
LITERATURE REVIEW

3.1 Graphene Anode Materials for Lithium-Ion Batteries

Fossil fuel resources in the world are being depleted day by day. After this depletion, it has become very popular to work on issues such as the generation and storage of electrical energy, which is likely to replace fossil fuels. One of the most important components to be developed for systems that produce and consume electrical energy is an advanced battery that can store the existing energy. Among the energy storage applications developed to date, the most efficient system is lithium-ion batteries. General information about lithium-ion batteries is given under the title of theoretical background. The most important issues in the development of lithium-ion battery cells are the development of the anode, cathode, and electrolyte that make up the battery. The subject examined within the scope of this thesis is the examination of the applications of graphene material produced by different methods in energy storage systems. In addition, negative electrodes (anode) produced from graphene synthesized within the scope of the thesis will be examined. The literature review of other studies conducted in this context is as follows:

Wang et al. in their study in 2009, produced an anode using graphene, which they synthesized by the modified hummers method. In the analysis, it was seen that the graphene anode exhibited a specific capacity of 945 mAh/g and a reversible capacity of 650 mAh/g in the first cycle. After 100 cycles, the capacity decreased to 460 mAh/g, but this value is higher than the capacity of standard graphite anodes. At the end of the study, it was concluded that the graphene sheets improved the cycling performance and lithium storage capability of the anode (G. Wang, Shen, et al., 2009).

Peichao et al. in their study in 2010, graphene sheets were synthesized from graphite powder by the rapid high thermal expansion method at nitrogen atmosphere. Later, they produced anode using this graphene they synthesized. The initial discharge and charge capacities of the anode are 2035 mAh/g and 1264 mAh/g, respectively. In

addition, the reversible capacity of the anode made of graphene sheets is 540 mAh/g. This value is higher than the previously reported graphene anodes (Lian et al., 2010b).

Lian et al. in their study in 2011, were able to increase the reversible capacity of the graphene doped anode materials they developed up to 1264 mAh/g at a current density of 100 mA/g. They revealed that the battery cell they prepared showed a reversible capacity value of 848 mAh/g at a current density of 100 mA/g after 40 charge-discharge cycles. These values show that the graphene doped anode exhibits excellent electrochemical performance for lithium-ion battery systems (Lian et al., 2010a).

Puttapati et al. in their study in 2018, anode production was carried out using solar energy-reduced graphene oxide. It exhibited a capacity of 1480 and 880 mAh/g, respectively, in the first charge-discharge cycle. At the end of the following 60 charge-discharge cycles, its specific capacity was found to be greater than 500 mAh/g. These results show that reduced graphene oxide can be an excellent alternative for anode applications (Kumar Puttapati et al., 2018).

Sun et al. in their study in 2017, they examined the anodic performance of graphite-reduced graphene oxide. In the analysis, it was observed that the interlayer spacing of graphite (d-spacing) was 0.335 nm on average, and the interlayer spacing of reduced graphene oxide was 0.374 nm on average. This difference can store more lithium ions in the reduced graphene oxide structure than graphite. In the light of this information, it has been shown that the LiC6 structures formed on the reduced graphene oxide anode can reach a specific capacity of approximately 917 mAh/g. This value obtained is almost 3 times the expected specific capacity (372 mAh/g) in a graphite anode (Y. Sun et al., 2017).

Petnikota et al. in their study in 2014, synthesized microwave-assisted few layers of graphene (FLG) from graphene oxide. FLG showed reversible capacity values of ~400 and ~250 mAh/g at 0.1 and 1C, respectively. It showed the maximum charge-discharge capacity below 0.3 V, where ideal anodic behavior was observed (Petnikota et al., 2014).

Guo et al. in their study in 2009, graphene nanosheets were synthesized with the help of rapid thermal expansion and ultrasonication after oxidation of pristine graphite. The anode they produced from the synthesized graphene exhibited a relatively high reversible capacity value of 672 mAh/g (P. Guo et al., 2009b).

Ahn et al. in their study in 2014, they synthesized morphology-controlled graphene nanosheets. They modified the method they developed so that graphite oxide (GO) has a higher oxide grade. As a result of this improvement, the d-spacing of GO increased from 0.87 nm to 0.92 nm. In addition, the O/C ratio in the structure of GO increased from 2.51 to 8.27. The graphene nanosheets produced by this method exhibited a discharge capacity of 1079 mAh/g and 1002 mAh/g after 50 cycles at a constant current of 40 mA/g (Ahn et al., 2014).

Standard graphite anodes used in lithium-ion batteries cannot provide high power density due to the slow diffusion rate of lithium ions. To eliminate this problem, Mukherjee et al. In their study in 2012, developed a graphene anode for lithium-ion batteries. Within the scope of the study, graphene was synthesized by reducing graphene oxide with photoflash and laser source. Thanks to this reduction process, pores and cracks were formed on the graphene structure. Thanks to these structural defects, the access of lithium ions to the underlying graphene layers is facilitated. It has been reported that after 1000 charge/discharge cycles at 40ºC, the anode continuously exhibits a capacity of ~156 mAh/g (Mukherjee et al., 2012).

As a result of the use of graphene as an anode material in all the studies summarized above, it has been clearly seen that it will exhibit superior performance compared to traditional graphitic anodes. However, although the majority of the studies are on the production of graphene by different methods, it is not exactly known how the differences in the production method will affect the use of graphene as an anode material. Within the scope of the thesis, the anode performance of graphene structures produced by different methods was analyzed with the help of characterization methods and the results were examined.

CHAPTER FOUR
EXPERIMENTAL PROCEDURE

4.1 Purpose

As reported in the previous sections, graphene can be produced by different methods. At the same time, when these graphene structures are used as anode material in lithium-ion batteries, they show superior properties compared to the traditional anode material graphite. Within the scope of this thesis, studies were carried out to determine the most suitable production method for graphene structures that can be used in lithium-ion batteries. Firstly, graphene synthesis was carried out with the help of top-down production methods using graphite raw material. Later, these graphene structures were used as working electrodes in the triple electrode system where a battery cell was simulated. In this way, it was tried to determine the anodic performance of graphene structures produced by different methods. At the same time, the produced graphene structures were evaluated with the help of structural, chemical, and morphological characterization methods.

4.2 Materials

In this section, supplier information and physical, chemical and electrical properties of the materials used in the production of graphene and electrodes are listed in Table 4.1

Table 4.1 Properties of materials used in experimental studies

Materials	**Supplier**	**Purity**	**Chemical Formula**
Sulfiric acid	Tekkim	95-98%	H_2SO_4
Hydrochloric acid	Tekkim	37%	HCl
N,N-Dimethylformamide (DMF)	Merck	99.8%	$HCON(CH_3)_2$
Phosphoric acid	Merck	85%	H_3PO_4
Potassium permanganate	Tekkim	99%	$KMnO_4$
Hydrogen peroxide	Tekkim	50%	H_2O_2
Hydrazine hydrate	Merck	80%	H_6N_2O
Graphite	Selen Kimya	85%	C
1-Methyl-2-pyrrolidone (NMP)	Merck	99.5%	C_5H_9NO
Poly (vinylidene fluoride) (PVDF)	Alfa Aesar	99%	$C_2H_2F_2$
Carbon black	Merck	99%	C

4.3 Methods

Purchased commercial flake graphite powder and rod were used for graphene production. Rapid thermal expansion, liquid phase exfoliation, electrolysis, and reduction of graphene oxide methods were used to synthesize graphene from flake graphite powder. Working electrodes to be used for electrochemical analysis were prepared using the samples obtained after graphene production.

Rapid thermal expansion is essentially an intermediate step for graphene production. In this process, powder graphite was first added into the sulfuric acid (H_2SO_4)-hydrochloric acid (HCl) mixture prepared at a ratio of 1:1.5 by volume and stirred for 4 hours. After the mixing process, distilled water (DW) was carefully added into the mixture and the reaction of the acid and graphite particles was stopped. Then, the mixture was filtered and the slurry was separated from the liquid phase and then washed 3 times with DW. After washing, the slurry form was dried at 80°C for 24 hours. The dried powder structure is called expandable graphite. The expandable

graphite structure was taken into a muffle furnace in a crucible and exposed to a temperature of about 1000°C for 30 seconds. During this process, the functional groups from the low number of acidic materials in the graphite structure evaporated and suddenly expanded the graphite. The structure obtained as a result of the rapid thermal expansion process is called expanded graphite or worm-like graphite (WLG). In addition, the WLG structure is also called worm-like graphene because it shows similar properties with graphene thanks to its large surface area and electrical conductivity in some applications.

In the liquid phase exfoliation method, WLG powder was taken into N,N-dimethylformamide (DMF) organic solvent and placed in an ultrasonic bath. The WLG/DMF ratio of the prepared solution is 2.5 mg/ml. Then, the solution prepared in the specified ratios was tried to exfoliate in the liquid phase with the help of ultrasonic sound waves in an ultrasonic bath for 72 hours. After ultrasonic treatment, the solution was centrifuged. Since the graphene particles in the solution in the centrifugation process are low weight, they accumulated at the top of the centrifuge tube. The heavy graphitic structures that have not yet turned into graphene precipitated at the bottom of the tube. Centrifugation was carried out at 4000 rpm for 20 minutes. After centrifugation, the slurry graphene structure collected from the upper part of the centrifuge tubes was dried in an oven at 80°C for 24 hours to obtain a powdered graphene structure.

The electrolysis method is also a kind of liquid-phase exfoliation method, but this method uses electrical energy and ion mobility instead of ultrasonic sound waves. The prepared electrolysis cell consists of a graphite rod cathode, a stainless-steel anode and an ionic conductivity electrolyte containing sulfuric acid (H_2SO_4). The concentration of the electrolyte prepared by using sulfuric acid and distilled water is 0.1 M. After the preparation of the electrolysis cell, the anode and cathode ends were connected to an external DC power source and a voltage of 10V was applied to the circuit. Electrolysis was continued until the part of the graphite rod in the solution completely exfoliated (approximately 2 hours). After the electrolysis process, the solution was sonicated for 2 hours in case the graphite structures remained in the structure. After sonication, the

solution was washed 3 times with distilled water with the help of the prepared vacuum filter system. After washing, it was centrifuged at 4000 rpm for 15 minutes to separate the graphene powders from the solution. The slurry graphene form obtained after centrifugation was dried at 80°C for 24 hours.

The modified Hummers method was used for the reduction of graphene oxide, which is another graphene production method. In this method, a mixture of sulfuric acid (H_2SO_4) and phosphoric acid (H_3PO_4) with a volume ratio of 9:1 was used as the oxidizing agent. Then, graphite powder was added to this prepared mixture at a rate of 133.3 ml/g and mixing was carried out. After mixing for about half an hour, potassium permanganate ($KMnO_4$) was added slowly, 5.85 times the amount of graphite added to the mixture. This solution was then subjected to magnetic stirring for 6 hours. After mixing, 0.5 ml/g of hydrogen peroxide (H_2O_2) was added dropwise into the solution in order to eliminate the excess $KMnO_4$ in the structure. A period of time was waited for the temperature to drop due to the exothermic reaction occurring during the addition of hydrogen peroxide. Then, the HCl-distilled water (DW) mixture prepared at a ratio of 1:3 by volume was added to the solution and then centrifuged at 4000 rpm for 15 minutes. In order to remove excess chemicals and other residues in the slurry form obtained in the centrifugation process, it was washed 4 times with an HCl-DW mixture. The washed GO solution was dried in an oven at 80°C for 24 hours to be powdered. In order to obtain graphene from the graphene oxide structure obtained at the end of the Hummers method, a reduction process was performed. For the reduction process, a reflux system was set up and 1mg/ml of GO was added to DW. Then, hydrazine hydrate (H_6N_2O) (1mL per 5mg of GO) was added to this mixture, which will perform the reduction process. Afterward, the solution was stirred for 6 hours and after mixing, it was washed with a vacuum filter system to obtain reduced graphene oxide (rGO). In addition, the codes of all samples produced were given in Table 4.2.

Table 4.2 Codes of all produced samples

Sample Name	Code
Graphite	Gr
Worm-like graphene	WLG
Liquid phase graphene	LPG
Electrolysis graphene	EG
Reduced Graphene Oxide	rGO

After the graphene samples were produced, graphene working electrodes were prepared to be used in the triple electrode system in order to perform electrochemical analysis. Firstly, aluminum plates of 7x8 mm size, on which the graphene will be coated, were cut. Later, the surfaces of these plates were made suitable for coating with the help of metallographic methods. Then, a copper cable was connected from one side of the plate to provide electrical conduction, and it was taken into molds and made ready for use in the triple-electrode system. In order to coat graphene structures on the working electrode, the coating slurry preparation recipe given in Table 4.3, which was created as a result of literature searches, was used. The sample image of the prepared anodes and the image of the triple electrode system is given in Fig. 4.1. After the relevant coatings were made on the working electrode, all samples were dried. As a result of the drying process, it was observed that a mud crack was formed in the anode structure containing the LPG coded graphene sample. It can be said that the functional groups that provide hydrophilic properties in the LPG structure are insufficient.

Table 4.3 Working electrode (anode) slurry recipe

Matrix Material (%)	**Active Material (Carbon Black) (%)**	**Binder (PVDF) (%)**	**Solvent (NMP) (g)**
Graphite, 80%	10%	10%	1.5
WLG, 80%	10%	10%	1.5
LPG, 80%	10%	10%	1.5
EG, 80%	10%	10%	1.5
rGO, 80%	10%	10%	1.5

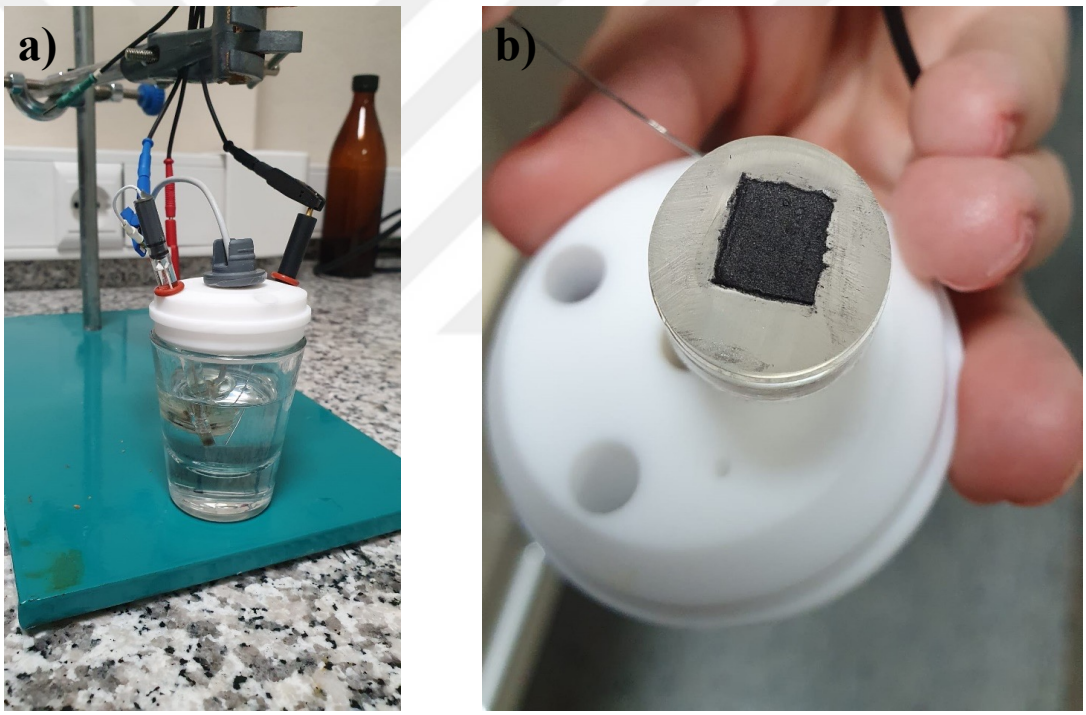


Figure 4.1 The image of (a) the triple electrode system and (b) the sample image of the prepared anodes (Personal Archive, 2021)

4.4 Materials Characterization

4.4.1 X-ray Diffraction

X-ray diffraction (XRD) analysis is the most widely used characterization method for analyzing the crystal structures of material forms such as bulk, powder, or thin film. From the data obtained as a result of XRD analysis, data such as crystal grain size, phase composition, tension, and crystallographic orientation can also be obtained with mathematical formulations. Basically, X-rays produced by an X-ray source are sent to the surface of the analyzed material at a certain angle. Then, the reflection angle (2θ) of the diffracted rays on the material is collected by the detector and processed. The graphene structures produced and the graphite structure, which is the raw material used for production, were also subjected to XRD analysis. Thermo Scientific's ARL X'TRA model XRD device, whose image is given in Fig. 4.2, was used for the analysis. Material samples were scanned with Cu-Kα (1.54185 Å) radiation at 40 kV and 40 mA. Scanning was carried out at room temperature at 2θ between 5°-90°, at a speed of 4°/min.



Figure 4.2 X-Ray Diffractometer analysis device, Thermoscientific ARL X'TRA (Personal archive, 2021)

4.4.2 Scanning Electron Microscopy

Scanning electron microscopy (SEM) analysis is a widely used characterization method for determining the surface morphology of solid samples. A high-energy and small-diameter electron beam is sent onto the sample to scan the surface. In addition to the morphological analysis, elemental analysis can also be performed using the radiation generated by the interaction between the electron beam and the material. As a result of the interaction of the electron beam with the material surface, secondary electrons (SE), backscattered electrons (BSE) and X-rays are produced. SE's are the electrons that emerge as a result of the interaction of the electrons sent from the source with the atoms on the sample surface. Thanks to these obtained SE's, the morphological image of the sample surface is created with high resolution. Since very small diameter electron beams are used during the analysis, 3D morphological images with a wide depth of field can be obtained. In SEM analysis, it is possible to obtain images magnified hundreds of thousands of times, depending on the device brand and model. Some predictions can be made about the elements on the surface, thanks to the BSEs that are reflected back by undergoing elastic collision from the electrons sent to the sample surface. Here, by evaluating together with the atomic number of the possible elements on the surface and the intensity of the BSE signals, an estimate can be made about the distribution of the elements on the material surface. At the same time, when the primary electrons hit the material surface, they can excite the electrons around the atoms on the surface. As a result of this interaction, electrons move between orbitals, move to an upper orbital, and then emit characteristic X-rays as they return to their orbitals. These emitted X-rays are collected by the detector and elemental analysis (composition and amount) of the sample is performed. The surface morphologies of graphene samples were analyzed with the help of SEs by applying 10 kV voltage with Zeiss, Gemini model SEM device, which is visualized in Fig. 4.3.



Figure 4.3 SEM analysis device, Zeiss-Gemini (Personal archive, 2021)

4.4.3 X-Ray Photoelectron Spectroscopy

X-ray photoelectron spectroscopy (XPS) analysis is a characterization method used to quantitatively determine the elemental composition, electronic and chemical state of materials. XPS analysis can be used for chemical analysis of the surfaces of materials. Basically, the x-rays produced by the X-ray source inside the device are sent to the material surface. These rays can receive data from about 1 nm to 10 nm depth of the material. All processes inside the XPS device are carried out under high vacuum conditions. In addition to surface chemistry analysis, it is also used to study the effects of ion beam etching, beam implantation, ultraviolet light or solutions, and the effects of mechanical deformation processes. In XPS analysis, elements with atomic number 3 (lithium, Li) or more can be analyzed. In order to make the elemental analysis of the graphene structures produced within the scope of the thesis, XPS analysis was performed with the A Thermo Scientific K-Alpha model device, the image of which is given in Fig. 4.4. The device, whose image is given, contains a monochromatic Al-Kα (1486.7 eV) X-ray source, which forms the basis of the analysis.



Figure 4.4 XPS analysis device, Thermo Scientific K-Alpha (Personal archive, 2021)

4.4.4 Raman Spectroscopy

Raman spectroscopy is a non-destructive characterization method that allows us to obtain detailed information about the chemical structure, crystallinity, phase, polymorphology, and molecular interaction of materials. The basis of the analysis is based on analyzing the interaction of light with chemical bonds in the material. In Raman analysis, the rays produced from a high-intensity laser source are sent onto the sample to interact and then the sample to reflect the incoming light. Since most of the light scattered from the material has the same wavelength as the laser source, it cannot provide useful information and is called the Rayleigh Scatter. However, a very small amount of light (about 0.0000001%) is scattered at different wavelengths depending on the chemical structure of the material, which is called the Raman Scatter. A spectrum is created by using the collected Raman scattering lights collected by the detector and this is called the Raman spectrum. By examining the peaks of the peaks in the Raman spectrum, C-C, C=C, N-O, C-H etc. such as individual bonds, molecular vibrations, lattice modes, polymer chain vibrations, etc. information about the subjects.

In order to determine the number of layers by examining the carbon bond structures of the graphene samples produced within the scope of the thesis, a monochromatic laser sourced Renishaw brand Raman spectroscopy device with a wavelength of 532 nm, whose image is given in Fig. 4.5, was used.



Figure 4.5 Renishaw Raman Spectroscopy device (Personal archive, 2021)

4.4.5 Electrochemical Measurements

Cyclic voltammetry (CV) is an important and widely used electroanalytical method in many areas of chemistry. It is a method that is generally used in areas such as examining redox processes, examining the stability of reaction products, obtaining qualitative information about electrode reaction mechanisms, examining charge transfer reactions between electrolyte ions and electrons from the electrode surface. Therefore, it is a very important method that can be used to examine the redox reaction, which plays an important role in the charge storage mechanism in the battery. Cyclic voltammetry, which takes place in a three-electrode electrochemical cell, is based on varying the applied potential in an electrode operating in both the forward and reverse directions (at a specified scanning rate) while observing the current. Cyclic voltammetry is a potentiodynamic electrochemical measurement in which the potential of the working electrode rises in the opposite direction to return to its initial potential.

These cycles can be repeated many times. The cyclic voltammogram gives the graph of current versus applied potential.

Impedance spectroscopy (EIS) is applicable for materials where ionic conduction predominates in electronic conduction. Examples of such systems are solid and liquid electrolytes, glasses, and polymers, although this technique is largely used for corrosion or electrochemical and characterization purposes in photoelectrochemical cells such as fuel cells, batteries, or solar devices. The EIS is based on the application of an alternating current (AC) voltage to the system under study and the analysis of the AC current (voltage) response as a function of frequency. It is usually performed using a potentiostat and a frequency response analyzer, and the measurement is taken relative to a fixed reference electrode of known potential.

CV and EIS analyzes made within the scope of the thesis were performed with the PalmSens 3 model potentiostat/galvanostat device given in Fig. 4.6. In the created triple-electrode system, Ag/AgCl was used as the reference electrode, platinum (Pt) as the counter electrode, and the graphene samples produced as the working electrode. The electrolyte used in the electrode system is a 5M lithium nitrate ($LiNO_3$) solution.

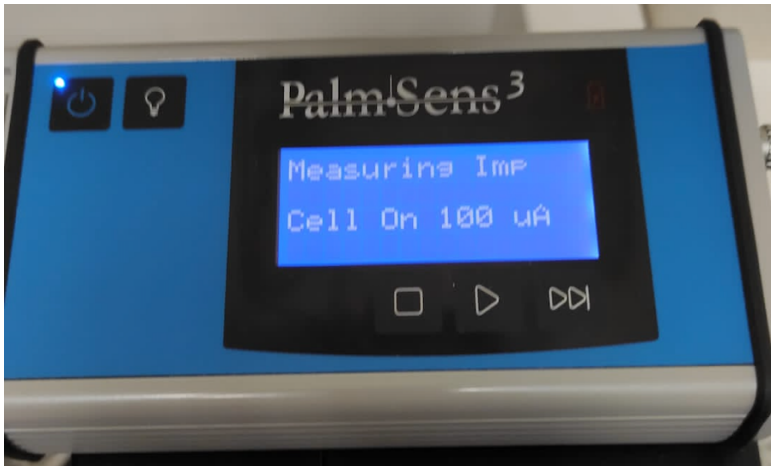


Figure 4.6 PalmSens 3 potentiostat/galvanostat device (Personal archive, 2021)

CHAPTER FIVE
RESULTS AND DISCUSSION

5.1 Structural Properties

XRD graphs of graphite and graphene samples are given in Fig. 5.1. In addition, 2θ diffraction angles and maximum peak intensities learned from these graphs are given in Table 5.1. The peaks of the XRD graph of the Gr-coded graphite raw material match with the standard XRD data of the graphite (JCPDS card, file no. 41-1487) (C. Ma et al., 2017). The characteristic XRD peak of graphite has a maximum intensity at 2θ =26º. XRD device analyzes according to Bragg's law. The formula for Bragg's law is nλ=2dsinθ. In this formula, n is the diffraction order, λ is the wavelength of the beam from the X-ray source, d is the interlayer spacing, and θ is the diffraction angle. In the XRD analysis made within the scope of the thesis, the n and λ values specified in Bragg's formula are constant, but the θ and d values vary according to the analyzed material. There is a negligible difference in the 2θ value for other samples except for rGO. This shows that graphite and graphene have similar crystal structures. In the rGO sample, a shift of 2θ was observed due to production. Here, the oxidation of graphite in rGO production increases the distance between graphite layers. According to Bragg's formula, if the distance d increases, the diffraction angle value will decrease and therefore there is a shift in the value of 2θ. When the peak intensities are compared in the XRD graphs, it can be said that the peak intensity decreases in the (002) plane corresponding to 2θ=26º, and the number of crystal structures oriented in the same direction decreases. At the same time, this decrease is a situation that shows that the weak van Der Waals bonds between graphite layers are broken and the structure becomes graphene by decreasing the number of layers.

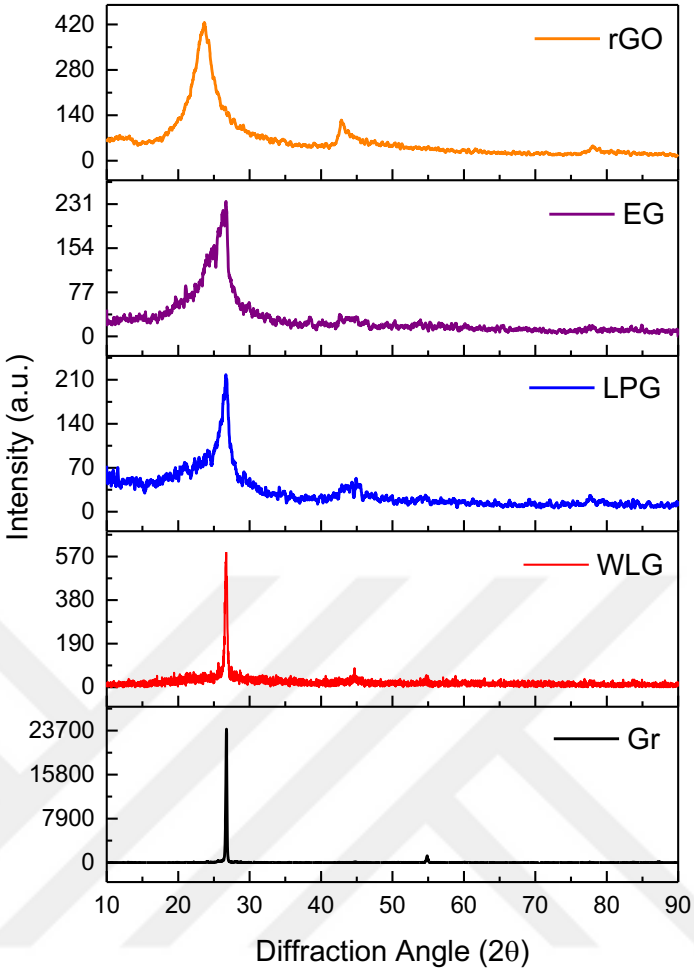


Figure 5.1 XRD graphs of graphite and graphene samples

Table 5.1 2θ diffraction angles and maximum intensities of XRD graphs

Samples	2θ (°)	Maximum Peak Intensity
Gr	26.76	23980
WLG	26.72	590
LPG	26.7	216.96
EG	26.74	226.66
rGO	23.58	421.98

5.2 Morphological Properties

SEM images of graphite and graphene samples are given in Fig. 5.2. The images in Fig. 5.2 (a) and (b) belong to the flake graphite powder used in the production of graphene. When these images are examined, it clearly shows that the graphite structure has a layered flake structure suitable for graphene production.

The images in Fig. 5.2 (c) and (d) belong to the WLG samples that emerged as a result of rapid thermal expansion, which is the preliminary stage of graphene production by the liquid-phase exfoliation method. As can be seen from these images, the flake graphite structure has expanded considerably with the effect of high temperature and the distance between its layers has increased. In addition, it is understood to have a worm-like appearance, matching the nomenclature of worm-like graphite or graphene.

Then, the graphene structure was obtained by separating the WLG samples into layers with the help of ultrasonic sound waves. The independent existence of layers of these produced graphene structures is clearly seen in Fig. 5.2 (e) and (f) images.

The images of the EG samples obtained as a result of the production of graphene by electrolysis, which is another production method, are given in Fig. 5.2 (g) and (h). When these images are examined, the wrinkled structure of the graphene sheets produced stands out. The reason for this wrinkling is the oxidizing effect of the sulfuric acid in the electrolyte used to produce the EG samples.

Fig. 5.2 (i) and (j) images belong to the graphene structures obtained as a result of the reduction of graphene oxide. When these images are examined, the presence of wrinkles, similar to the EG samples, is striking. The main reason for this similarity is the use of oxidizing agents as in the electrolysis method.

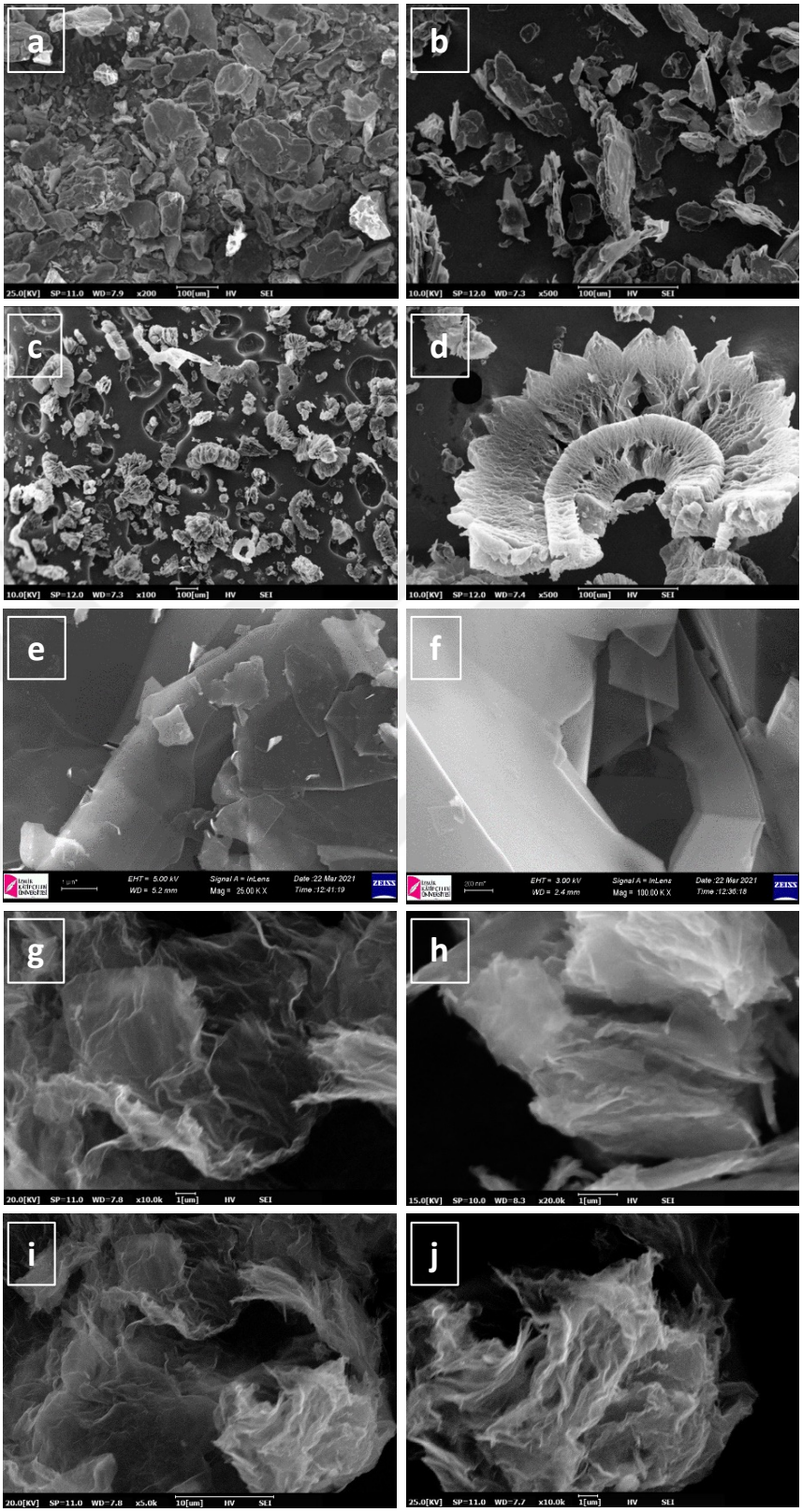


Figure 5.2 Sem images of graphite and graphene samples

5.3 Chemical Properties

XPS graphs of graphite and graphene samples are given in Fig. 5.3. In addition, the binding energies and percent elemental distribution data of the elements shown in the graphics are given in Table 5.2. When the graph of the Gr coded sample is examined, it is seen that carbon (C), oxygen (O), silicon (Si), iron (Fe), and magnesium (Mg) elements are present in the graphite structure. Normally, there is no element other than C in a high purity Gr sample. However, since the raw material used is of mineral origin, there are other elements accompanying element C. In addition, it is another reason that increases the presence of the element O, especially in cases such as the oxidation or humidity of the Gr sample due to external environmental conditions.

When the graph of the WLG coded sample is examined, it is seen that there are C, O, Si, and N elements. The presence of the C1s general carbon peak with a binding energy of 284.7 eV is consistent with the high amount of C element in the raw material(Johra et al., 2014). Oxygen (O) element, on the other hand, is in the structure as a result of environmental oxidation and production. The reason for the existence of this element is the intrinsic structure of the raw material and the oxidizing effect of the chemical agents used during WLG production. The presence of the Si element, which is one of the other Si and N elements whose existence is seen as a result of the analysis, is due to the intrinsic structure of the raw material. The N element, on the other hand, is an undesirable element but may have arisen due to production origin or contamination of the analysis environment.

When the graphs of LPG, EG, and rGO samples are examined, there is no peak indicating the presence of any element other than the general C peak and the O element peak. The main difference between the chemical structures of these three samples is that they have different amounts of O element from production. O element amounts of LPG, EG, and rGO samples are 1.77%, 3.27%, and 11.13%, respectively. The main reason why the oxygen level of rGO is higher than other samples is the strong oxidizing agents used during production.

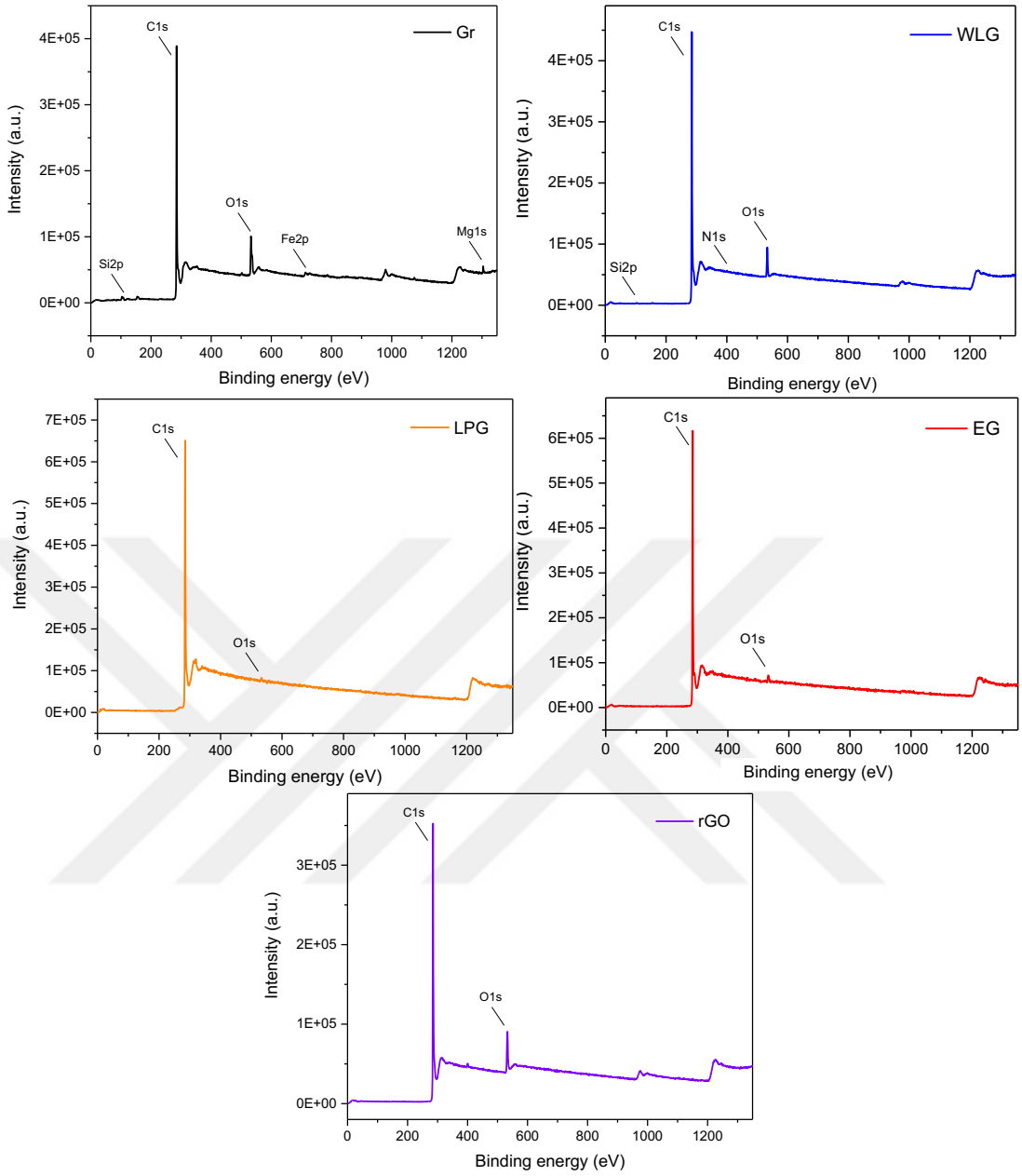


Figure 5.3 XPS spectra of graphite and graphene samples

Table 5.2 The binding energies, FWHM values, and detailed chemical properties of the peaks of the elements in graphite and graphene samples

Sample Code	Element	Peak (eV)	FWHM	Elemental Distribution (%)
Gr	C1s	285.17	2.21	76.77
Gr	O1s	532.53	2.21	13.63
Gr	Fe2p	713.31	6.52	3.39
Gr	Si2p	103.4	2.5	5.06
Gr	Mg1s	1304.19	2.48	1.14
WLG	C1s	285.06	2.3	89.9
WLG	O1s	533.2	3.2	7.61
WLG	N1s	400.49	3.74	0.88
WLG	Si2p	103.84	5.22	1.61
LPG	C1s	285	2.59	98.23
LPG	O1s	532.87	4.12	1.77
EG	C1s	285.02	2.33	96.73
EG	O1s	532.75	4.87	3.27
rGO	C1s	285.09	2.47	88.87
rGO	O1s	532.82	3.81	11.13

5.4 Raman Analysis

Raman analysis is one of the most important components of studies on graphene. It is used to determine the number of layers and direction, doping effect, structural defect and disorder, functional groups, electric and magnetic field (Ferrari & Basko, 2013). The most used data when examining the Raman spectrum are the intensity values of the 2D and G peaks. The ratio of 2D peak to G peak (I_{2D}/I_G) shows the difference between graphene and graphite and is also the most powerful data used to predict the number of layers of graphene (J. bin Wu et al., 2018).

Raman spectra of graphite and graphene (except rGO) samples are given in Fig. 5.4. The I_{2D} and I_G values and I_{2D}/I_G ratios obtained from these spectra are given in Table 5.3.

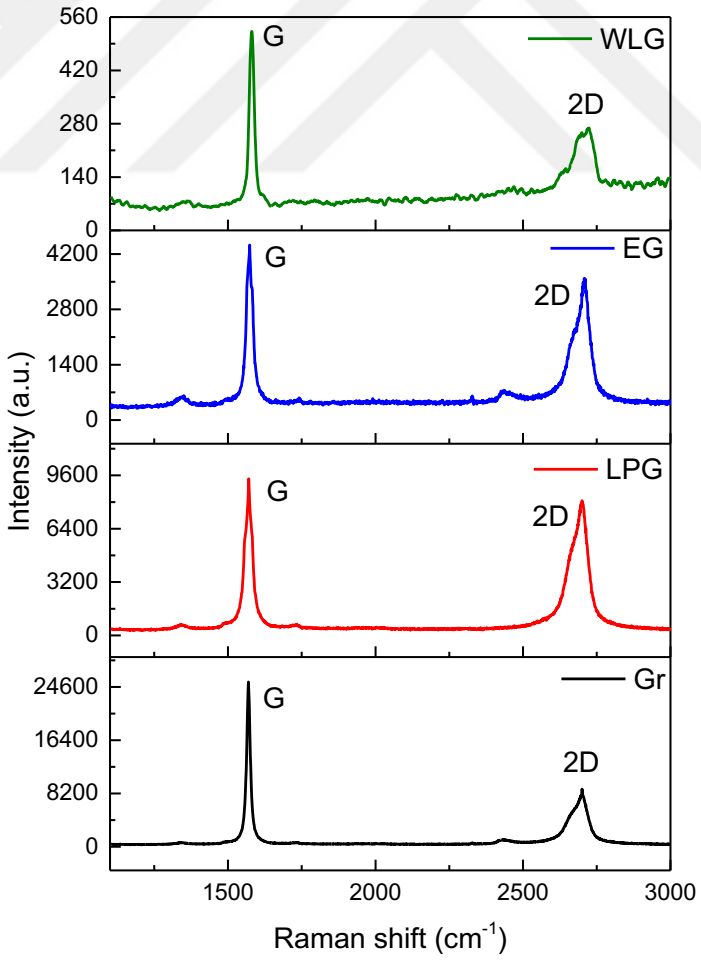


Figure 5.4 Raman graphs of graphite and graphene samples

Table 5.3 I_{2D} and I_G data and I_{2D}/I_G ratios of samples

Samples	2D	G	I_{2D}/I_G
Gr	8863.11	25356.89	0.35
WLG	268.08	522.37	0.51
LPG	8079.12	9394.46	0.86
EG	3587.59	4428.22	0.81

It is expected that the 2D peak intensity will decrease as one moves from the graphite raw material to the graphene structure. The I2D/IG ratio is 2 and above for single-layer graphene, 1-2 for double-layer graphene, 0.8-1 for few-layer graphene, and 0.5-0.8 for multilayer graphene (J. bin Wu et al., 2018). In the light of this information, it can be said that LPG and EG samples fall into the multilayer graphene classification. These results obtained in Raman analysis also support the layered graphene structures in SEM images.

5.5 Electrochemical Measurements

CV analysis of the anodes prepared using the produced graphene samples was performed at a scanning speed of 5 mV/s and was repeated 5 times for each sample. Graphics prepared using CV analysis data are given in Fig. 5.5. In the triple-electrode system used in the CV analysis, Ag/AgCl was used as the reference electrode, platinum (Pt) as the counter electrode, and graphene structures coated with the anode slurry, the recipe of which is given in Table 4.2, as the working electrode. When the graphics are examined, the oxidation-reduction cycles of the anode structures prepared using Gr, WLG, EG, and rGO coded samples are seen. The completion of the cycles during the applied 5 cycles shows that the lithiation-delithiation reactions can take place on the produced anode. Ideally, the shape that appears on the CV graph is expected to be rectangular. However, this shape may vary depending on the type of electrolyte used in the triple electrode system. Since the ionic lithium solution, which does not contain complex compounds, is used in our analysis, the shape of the graphs is close to ideal. In the light of this information, it can be said that except for the EG sample, other samples exhibit cyclic voltammetry close to ideal. Another important conclusion that

can be drawn from the CV analysis is the stability of the cycles. In general, after the first cycle, it is expected that other cycles will stabilize and provide the same cycle. In this way, the cyclic stability of the anode can be determined by making hundreds of cycles. This will allow us to comment on how long the anode can provide the desired physical conditions. When the anode samples produced within the scope of the thesis are examined, it can be said that the cyclic stability of the Gr and WLG coded samples is better. Although there is a rectangular loop in the rGO sample, the current value decreases slightly at the end of each repeated cycle. In this case, it shows us that the stability of the reactions on the rGO anode is lower than the other samples.

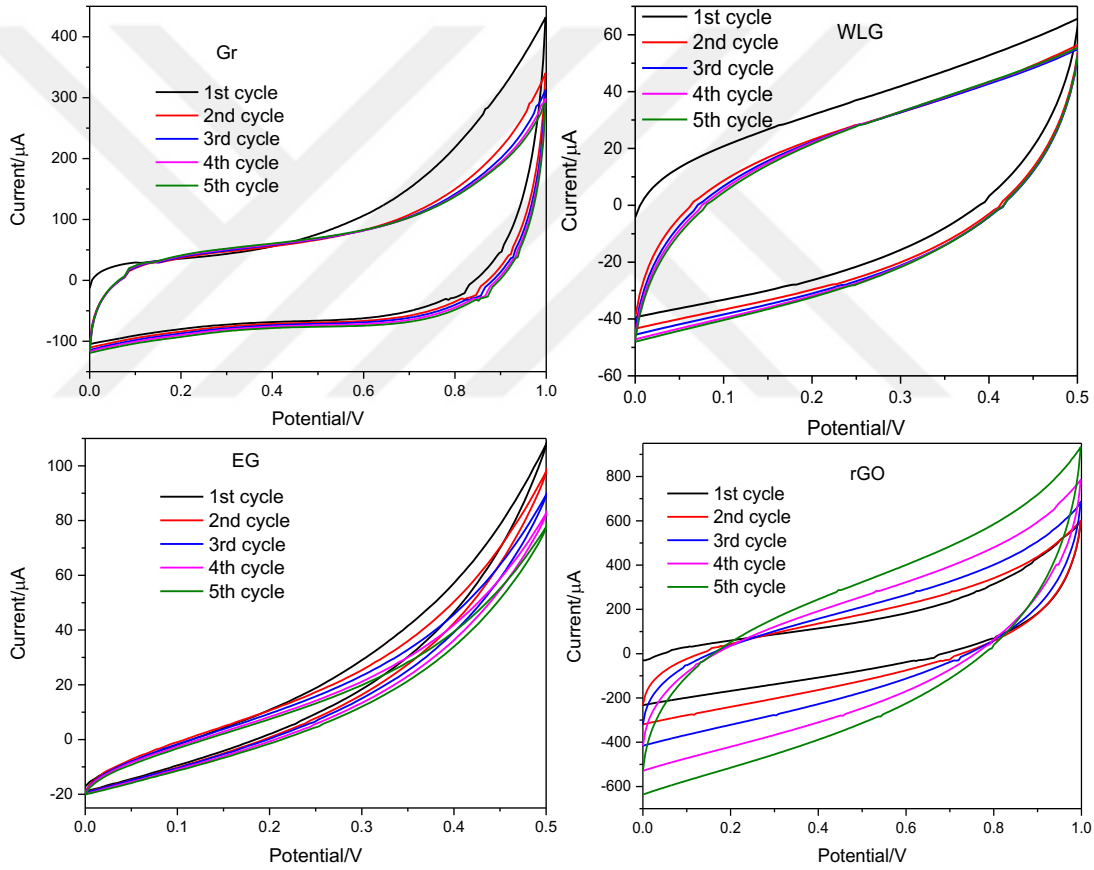


Figure 5.5 CV graphs of graphite and graphene samples

Another electrochemical analysis performed on the produced anodes is EIS. It is an electrochemical technique to measure the impedance of a system's independence of the AC potentials frequency. When the EIS analysis results in Fig. 5.6 are examined, the peak image formed in the region outside the linear part of the curve allows us to

have an idea about the resistance of the working electrode. The width of the semicircular formation seen in this section is proportional to the impedance of the electrode, and the resistance increases as the width increases. When the curve of the EG sample is examined, it is seen that the circular structure is extremely large. It can be said that the resistance of this situation is quite high compared to other samples. The fact that the Gr and WLG coded samples have a more linear appearance compared to the other samples indicates that the resistance is low. The low resistance is also an indication of rapid electric current. Since the resistance is low, it also increases the anode performance as it ensures that the electricity flow is fast.

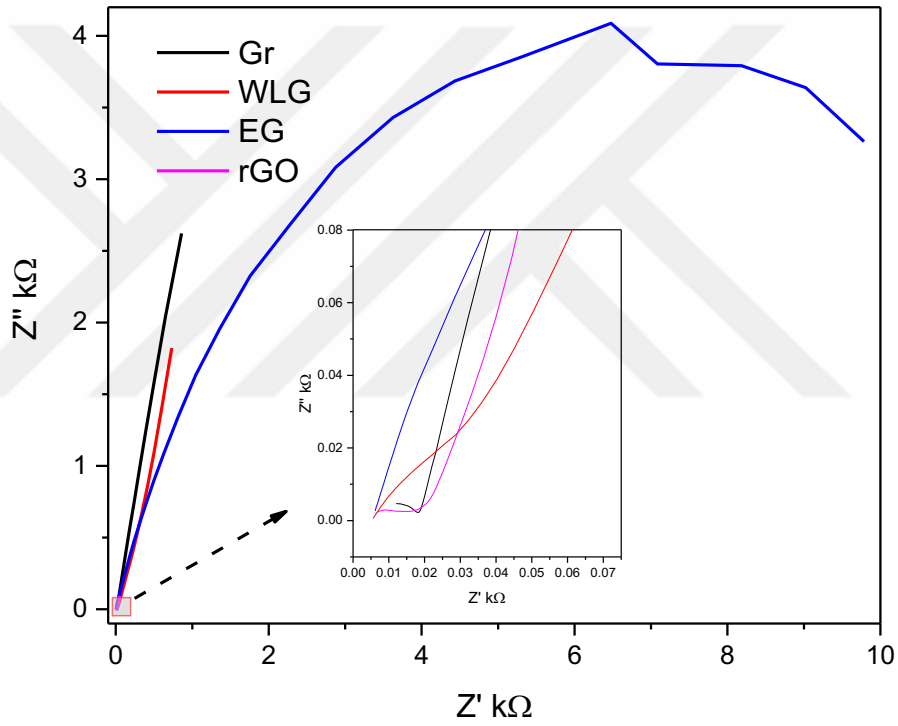


Figure 5.6 EIS analysis graphs of samples

CHAPTER SIX
CONCLUSION AND FUTURE WORKS

Graphene production has been carried out with different methods and its anodic performances have been studied successfully. The results obtained within the scope of the thesis can be summarized as follows;

1. Graphene production with different methods was examined and as a result of the studies, graphene production was carried out successfully with these methods.
2. Graphene samples showed lower intensity in XRD results compared to the raw material graphite, similar to the literature samples.
3. All graphene structures (although the ratio varies) contain oxygen, unlike the ideal graphene structure.
4. As a result of the production methods discussed in the SEM images, it was observed that the graphite layers separated from each other and became graphene.
5. In accordance with the literature, the producibility of few-layer graphene was confirmed in the results of the Raman analysis.
6. The graphene samples produced were converted into anodes and their electrochemical results were examined.
7. In the CV analysis results, it has been shown that all samples except LPG have a high probability of being used as anode material and can provide stable cycling.
8. As a result of EIS analysis, it has been seen that the resistance of the anodes produced is low, except for the EG sample, and it is suitable to be used as an anode material.

Parametric studies can be performed to produce higher quality (electrical, hydrophilicity, high surface area, etc.) graphene samples. In addition, the anode materials produced are converted into lithium-ion battery cells storage capacity, energy density, etc. detailed investigations can be made.

REFERENCES

AbdelHamid, A. A., Yang, X., Yang, J., Chen, X., & Ying, J. Y. (2016). Graphene-wrapped nickel sulfide nanoprisms with improved performance for Li-ion battery anodes and supercapacitors. *Nano Energy*, *C* (26), 425–437.

Abhervé, A., Mañas-Valero, S., Clemente-León, M., & Coronado, E. (2015). Graphene related magnetic materials: micromechanical exfoliation of 2D layered magnets based on bimetallic anilate complexes with inserted [FeIII(acac2-trien)] + and [FeIII(sal2-trien)] + molecules. *Chemical Science*, *6*(8), 4665–4673.

Ahn, W., Song, H. S., Park, S. H., Kim, K. B., Shin, K. H., Lim, S. N., & Yeon, S. H. (2014). Morphology-controlled graphene nanosheets as anode material for lithium-ion batteries. *Electrochimica Acta*, *132*, 172–179.

Al Faruque, M. A., Salauddin, M., Raihan, M. M., Chowdhury, I. Z., Ahmed, F., & Shimo, S. S. (2021). Bast fiber reinforced green polymer composites: a review on their classification, properties, and applications. *Journal of Natural Fibers*, 1-16.

Allen, M. J., Tung, V. C., & Kaner, R. B. (2009). Honeycomb carbon: A review of graphene. *Chemical Reviews*, *110*(1), 132–145.

Amatucci, G., & Tarascon, J.-M. (2002). Optimization of insertion compounds such as LiMn2O4 for Li-ion batteries. *Journal of the Electrochemical Society*, *149*(12), K31–K46.

Anand, A., Ghosh, S. K., Fulmali, A. O., & Prusty, R. K. (2021). Enhanced barrier, mechanical and viscoelastic properties of graphene oxide embedded glass fibre/epoxy composite for marine applications. *Construction and Building Materials*, *268*, 121784.

Arheimer, B. (2016). The active liquid Earth-importance of temporal and spatial variability. *Geophysical Research Abstracts*, *18*, 2016–17409.

Armand, M., & Touzain, P. (1977). Graphite intercalation compounds as cathode materials. *Materials Science and Engineering*, *31*(C), 319–329.

Arnold, G., Garche, J., Hemmer, R., Ströbele, S., Vogler, C., & Wohlfahrt-Mehrens, M. (2003). Fine-particle lithium iron phosphate LiFePO4 synthesized by a new low-cost aqueous precipitation technique. *Journal of Power Sources*, *119–121*, 247–251.

Ayeb, A., Otten, W. M., Mank, A. J. G., & Notten, P. H. L. (2006). The hydrogen evolution and oxidation kinetics during overdischarging of sealed Nickel-metal hydride batteries. *Journal of The Electrochemical Society*, *153*(11), A2055.

Berger, C., Song, Z., Li, X., Wu, X., Brown, N., Naud, C., Mayou, D., Li, T., Hass, J., Marchenkov, A. N., Conrad, E. H., First, P. N., & de Heer, W. A. (2006). Electronic confinement and coherence in patterned epitaxial graphene. *Science (New York, N.Y.)*, *312*(5777), 1191–1196.

Bobrinetskiy, I. I., & Knezevic, N. Z. (2018). Graphene-based biosensors for on-site detection of contaminants in food. *Analytical Methods*, *10*(42), 5061–5070.

Boehm, H. P., Clauss, A., Fischer, G. O., & Hofmann, U. (1962). Das adsorptionsverhalten sehr dünner Kohlenstoff-Folien. *Zeitschrift Für Anorganische Und Allgemeine Chemie*, *316*(3–4), 119–127.

Bosch-Navarro, C., Coronado, E., Martí-Gastaldo, C., Sánchez-Royo, J. F., & Gómez, M. G. (2012). Influence of the pH on the synthesis of reduced graphene oxide under hydrothermal conditions. *Nanoscale*, *4*(13), 3977–3982.

Bradley, T. H., & Frank, A. A. (2009). Design, demonstrations and sustainability impact assessments for plug-in hybrid electric vehicles. *Renewable and Sustainable Energy Reviews*, *13*(1), 115–128.

Bruce, P. G., Freunberger, S. A., Hardwick, L. J., & Tarascon, J. M. (2011). Li–O2 and Li–S batteries with high energy storage. *Nature Materials*, *11*(1), 19–29.

Cai, Z., Faruque, M. A. al, Kiziltas, A., Mielewski, D., & Naebe, M. (2021). Sustainable lightweight insulation materials from textile-based waste for the automobile industry. *Materials*, *14*(5), 1241.

Chen, K., Wang, Q., Niu, Z., & Chen, J. (2018). Graphene-based materials for flexible energy storage devices. *Journal of Energy Chemistry*, *27*(1), 12–24.

Choi, W., Lahiri, I., Seelaboyina, R., & Kang, Y. S. (2010). Synthesis of graphene and its applications: a review. *Critical Reviews in Solid State and Materials Sciences, 35*(1), 52-71.

Chung, S. Y., Bloking, J. T., & Chiang, Y. M. (2002). Electronically conductive phospho-olivines as lithium storage electrodes. *Nature Materials, 1*(2), 123–128.

Coraux, J., N'Diaye, A. T., Busse, C., & Michely, T. (2008). Structural coherency of graphene on Ir(111). *Nano Letters*, *8*(2), 565–570.

Cui, G., Bi, Z., Zhang, R., Liu, J., Yu, X., & Li, Z. (2019). A comprehensive review on graphene-based anti-corrosive coatings. *Chemical Engineering Journal*, *373*, 104–121.

Cui, G., Cheng, Y., Liu, C., Huang, K., Li, J., Wang, P., Duan, X., Chen, K., Liu, K., & Liu, Z. (2020). Massive growth of graphene quartz fiber as a multifunctional electrode. *ACS Nano*, *14*(5), 5938–5945.

Cui, X., Zhang, C., Hao, R., & Hou, Y. (2011). Liquid-phase exfoliation, functionalization and applications of graphene. *Nanoscale*, *3*(5), 2118–2126.

Dato, A., Radmilovic, V., Lee, Z., Phillips, J., & Frenklach, M. (2008). Substrate-free gas-phase synthesis of graphene sheets. *Nano Letters*, *8*(7), 2012–2016.

Datta, M. K., Maranchi, J., Chung, S. J., Epur, R., Kadakia, K., Jampani, P., & Kumta, P. N. (2011). Amorphous silicon-carbon based nano-scale thin film anode materials for lithium ion batteries. *Electrochimica Acta*, *56*(13), 4717–4723.

Delmas, C., Saadoune, I., & Rougier, A. (1993). The cycling properties of the LixNi1−yCoyO2 electrode. *Journal of Power Sources*, *44*(1–3), 595–602.

Díez-Pascual, A. M., Sánchez, J. A. L., Capilla, R. P., & Díaz, P. G. (2018). Recent developments in graphene/polymer nanocomposites for application in polymer solar cells. *Polymers*, *10*(2), 217.

Doh, C. H., Han, B. C., Jin, B. S., & Gu, H. B. (2011). Structures and formation energies of Li_xC_6 (x=1-3) and its homologues for lithium rechargeable batteries. *Bulletin of the Korean Chemical Society*, *32*(6), 2045–2050.

Endo, M., Kim, C., Nishimura, K., Fujino, T., & Miyashita, K. (2000). Recent development of carbon materials for Li ion batteries. *Carbon*, *38*(2), 183–197.

Ferrari, A. C., & Basko, D. M. (2013). Raman spectroscopy as a versatile tool for studying the properties of graphene. *Nature Nanotechnology*, *8*(4), 235–246.

Gao, Y. (2017). Graphene and Polymer Composites for Supercapacitor Applications: a Review. *Nanoscale Research Letters*, *12*(1), 1–17.

Geim, A. K., & Kim, P. (2008). Carbon wonderland. *Scientific American*, *298*(4), 90–97.

Geim, A. K., & Novoselov, K. S. (2007). The rise of graphene. *Nature Materials 2007 6:3*, *6*(3), 183–191.

Grosjean, C., Herrera Miranda, P., Perrin, M., & Poggi, P. (2012). Assessment of world lithium resources and consequences of their geographic distribution on the expected development of the electric vehicle industry. *Renewable and Sustainable Energy Reviews*, *16*(3), 1735–1744.

Gruber, P. W., Medina, P. A., Keoleian, G. A., Kesler, S. E., Everson, M. P., & Wallington, T. J. (2011). Global lithium availability. *Journal of Industrial Ecology*, *15*(5), 760–775.

Gu, P., Cai, R., Zhou, Y., & Shao, Z. (2010). Si/C composite lithium-ion battery anodes synthesized from coarse silicon and citric acid through combined ball milling and thermal pyrolysis. *Electrochimica Acta*, *55*(12), 3876–3883.

Gummow, R. J., & Thackeray, M. M. (1992). Lithium-cobalt-nickel-oxide cathode materials prepared at 400°C for rechargeable lithium batteries. *Solid State Ionics*, *53–56*(PART 1), 681–687.

Guo, P., Song, H., & Chen, X. (2009a). Electrochemical performance of graphene nanosheets as anode material for lithium-ion batteries. *Electrochemistry Communications, 11*(6), 1320-1324.

Guo, P., Song, H., & Chen, X. (2009b). Electrochemical performance of graphene nanosheets as anode material for lithium-ion batteries. *Electrochemistry Communications, 11*(6), 1320-1324.

Guo, S., & Dong, S. (2011). Graphene nanosheet: synthesis, molecular engineering, thin film, hybrids, and energy and analytical applications. *Chemical Society Reviews*, *40*(5), 2644–2672.

Gwon, H., Hong, J., Kim, H., Seo, D. H., Jeon, S., & Kang, K. (2014). Recent progress on flexible lithium rechargeable batteries. *Energy & Environmental Science*, *7*(2), 538–551.

Hariprakash, B., Shukla, A. K., & Venugoplan, S. (2009). Secondary batteries – nickel systems | nickel–metal hydride: overview. *Encyclopedia of Electrochemical Power Sources*, 494–501.

Herle, P. S., Ellis, B., Coombs, N., & Nazar, L. F. (2004). Nano-network electronic conduction in iron and nickel olivine phosphates. *Nature Materials*, *3*(3), 147–152.

Hernandez, Y., Nicolosi, V., Lotya, M., Blighe, F. M., Sun, Z., De, S., McGovern, I. T., Holland, B., Byrne, M., Gun'ko, Y. K., Boland, J. J., Niraj, P., Duesberg, G., Krishnamurthy, S., Goodhue, R., Hutchison, J., Scardaci, V., Ferrari, A. C., & Coleman, J. N. (2008). High-yield production of graphene by liquid-phase exfoliation of graphite. *Nature Nanotechnology*, *3*(9), 563–568.

Hu, X., Li, J., & Bai, Y. (2017). Fabrication of high strength graphene/regenerated silk fibroin composite fibers by wet spinning. *Materials Letters*, *C*(194), 224–226.

Hu, Y., & Sun, X. (2014). Flexible rechargeable lithium ion batteries: advances and challenges in materials and process technologies. *Journal of Materials Chemistry A*, *2*(28), 10712–10738.

Huang, H., Su, S., Wu, N., Wan, H., Wan, S., Bi, H., & Sun, L. (2019). Graphene-based sensors for human health monitoring. *Frontiers in Chemistry*, *7*(JUN), 399.

Iqbal, A. A., Sakib, N., Iqbal, A. K. M. P., & Nuruzzaman, D. M. (2020). Graphene-based nanocomposites and their fabrication, mechanical properties and applications. *Materialia*, *12*, 100815.

Jiao, L., Wang, X., Diankov, G., Wang, H., & Dai, H. (2010). Facile synthesis of high-quality graphene nanoribbons. *Nature Nanotechnology*, *5*(5), 321–325.

Jiao, L., Zhang, L., Wang, X., Diankov, G., & Dai, H. (2009). Narrow graphene nanoribbons from carbon nanotubes. *Nature*, *458*(7240), 877–880.

Jin, C., Wang, H. T., Liu, Y. N., Kang, X. H., Liu, P., Zhang, J. N., Jin, L. N., Bian, S. W., & Zhu, Q. (2018). High-performance yarn electrode materials enhanced by surface modifications of cotton fibers with graphene sheets and polyaniline nanowire arrays for all-solid-state supercapacitors. *Electrochimica Acta*, *270*, 205–214.

Johansson, B. (2013). A broadened typology on energy and security. *Energy*, *53*, 199–205.

Johnson, C. S., Kim, J. S., Lefief, C., Li, N., Vaughey, J. T., & Thackeray, M. M. (2004). The significance of the Li2MnO3 component in 'composite' xLi2MnO3·(1−x)LiMn0.5Ni0.5O2 electrodes. *Electrochemistry Communications*, *10*(6), 1085–1091.

Johra, F. T., Lee, J. W., & Jung, W. G. (2014). Facile and safe graphene preparation on solution based platform. *Journal of Industrial and Engineering Chemistry*, *20*(5), 2883–2887.

Kauling, A. P., Seefeldt, A. T., Pisoni, D. P., Pradeep, R. C., Bentini, R., Oliveira, R. V. B., Novoselov, K. S., & Castro Neto, A. H. (2018). The worldwide graphene flake production. *Advanced Materials*, *30*(44), 1803784.

Khan, M., Tahir, M. N., Adil, S. F., Khan, H. U., Siddiqui, M. R. H., Al-Warthan, A. A., & Tremel, W. (2015). Graphene based metal and metal oxide nanocomposites: synthesis, properties and their applications. *Journal of Materials Chemistry A*, *3*(37), 18753–18808.

Kim, H. J., Krishna, T. N. V., Zeb, K., Rajangam, V., Muralee Gopi, C. V. V., Sambasivam, S., Raghavendra, K. V. G., & Obaidat, I. M. (2020). A comprehensive review of Li-ion battery materials and their recycling techniques. *Electronics, 9*, 1161.

Kim, K. S., Zhao, Y., Jang, H., Lee, S. Y., Kim, J. M., Kim, K. S., Ahn, J. H., Kim, P., Choi, J. Y., & Hong, B. H. (2009). Large-scale pattern growth of graphene films for stretchable transparent electrodes. *Nature*, *457*(7230), 706–710.

Kosynkin, D. v., Higginbotham, A. L., Sinitskii, A., Lomeda, J. R., Dimiev, A., Price, B. K., & Tour, J. M. (2009). Longitudinal unzipping of carbon nanotubes to form graphene nanoribbons. *Nature*, *458*(7240), 872–876.

Kucinskis, G., Bajars, G., & Kleperis, J. (2013). Graphene in lithium ion battery cathode materials: A review. *Journal of Power Sources*, *240*, 66–79.

Kumar Puttapati, S., Gedela, V., S S Srikanth, V. v, Reddy, M. v, Adams, S., & R Chowdari, B. v. (2034). Unique reduced graphene oxide as efficient anode material in Li ion battery. *Bulletin of Materials Science*, *41*, 53.

Kumar, A., Sharma, K., & Dixit, A. R. (2019). A review of the mechanical and thermal properties of graphene and its hybrid polymer nanocomposites for structural applications. *Journal of Materials Science*, *54*(8), 5992–6026.

Kwon, S. J., Kim, C. W., Jeong, W. T., & Lee, K. S. (2004). Synthesis and electrochemical properties of olivine LiFePO4 as a cathode material prepared by mechanical alloying. *Journal of Power Sources*, *137*(1), 93–99.

Lang, B. (1975). A LEED study of the deposition of carbon on platinum crystal surfaces. *Surface Science*, *53*(1), 317–329.

Lee, C., Wei, X., Kysar, J. W., & Hone, J. (2008). Measurement of the elastic properties and intrinsic strength of monolayer graphene. *Science (New York, N.Y.)*, *321*(5887), 385–388.

Li, J., Martin, I., Büttiker, M., -, al, MacDonald, A. H., Jung, J., Zhang -, F., Köster, J., Novoselov, K. S., & Castro Neto, A. H. (2012). Two-dimensional crystals-based heterostructures: materials with tailored properties. *Physica Scripta*, *2012*(T146), 014006.

Li, X., Cai, W., Colombo, L., & Ruoff, R. S. (2009). Evolution of graphene growth on Ni and Cu by carbon isotope labeling. *Nano Letters*, *9*(12), 4268–4272.

Li, X., Wang, X., Zhang, L., Lee, S., & Dai, H. (2008). Chemically derived, ultrasmooth graphene nanoribbon semiconductors. *Science (New York, N.Y.)*, *319*(5867), 1229–1232.

Li, X., Zhang, G., Bai, X., Sun, X., Wang, X., Wang, E., & Dai, H. (2008). Highly conducting graphene sheets and Langmuir–Blodgett films. *Nature Nanotechnology*, *3*(9), 538–542.

Li, X., Zhu, Y., Cai, W., Borysiak, M., Han, B., Chen, D., Piner, R. D., Colomba, L., & Ruoff, R. S. (2009). Transfer of large-area graphene films for high-performance transparent conductive electrodes. *Nano Letters*, *9*(12), 4359–4363.

Li, Y., Song, J., & Yang, J. (2014). A review on structure model and energy system design of lithium-ion battery in renewable energy vehicle. *Renewable and Sustainable Energy Reviews*, *37*, 627–633.

Lian, P., Zhu, X., Liang, S., Li, Z., Yang, W., & Wang, H. (2010a). Large reversible capacity of high quality graphene sheets as an anode material for lithium-ion batteries. *Electrochimica Acta*, *12*(55), 3909–3914.

Liang, Y., Zhao, C.-Z., Yuan, H., Chen, Y., Zhang, W., Huang, J.-Q., Yu, D., Liu, Y., Titirici, M.-M., Chueh, Y.-L., Yu, H., & Zhang, Q. (2019). A review of rechargeable batteries for portable electronic devices. *InfoMat*, *1*(1), 6–32.

Lim, L., Liu, Y., Liu, W., Tjandra, R., Rasenthiram, L., Chen, Z., & Yu, A. (2017). All-in-one graphene based composite fiber: Toward wearable supercapacitor. *ACS Applied Materials and Interfaces*, *9*(45), 39576–39583.

Liu, J., Poh, C. K., Zhan, D., Lai, L., Lim, S. H., Wang, L., Liu, X., Gopal Sahoo, N., Li, C., Shen, Z., & Lin, J. (2013). Improved synthesis of graphene flakes from the multiple electrochemical exfoliation of graphite rod. *Nano Energy*, *2*(3), 377–386.

Liu, Y., Li, X., Fan, L., Li, S., Maleki Kheimeh Sari, H., & Qin, J. (2019). A review of carbon-based materials for safe lithium metal anodes. *Frontiers in Chemistry*, *7*, 721.

Liu, Z., Robinson, J. T., Sun, X., & Dai, H. (2008). PEGylated nanographene oxide for delivery of water-insoluble cancer drugs. *Journal of the American Chemical Society*, *130*(33), 10876–10877

Lu, J., Yang, J. X., Wang, J., Lim, A., Wang, S., & Loh, K. P. (2009). One-pot synthesis of fluorescent carbon nanoribbons, nanoparticles, and graphene by the exfoliation of graphite in ionic liquids. *ACS Nano*, *3*(8), 2367–2375.

Lu, X., Yu, M., Huang, H., & Ruoff, R. S. (1999). Tailoring graphite with the goal of achieving single sheets. *Nanotechnology*, *10*, 269–272.

Ma, C., Yang, K., Wang, L., & Wang, X. (2017). Facile synthesis of reduced graphene oxide/Fe3O4 nanocomposite film. *Journal of Applied Biomaterials and Functional Materials*, *15*, 1–6.

Ma, J., Shen, W., & Yu, F. (2017). Graphene-enhanced three-dimensional structures of MoS2 nanosheets as a counter electrode for Pt-free efficient dye-sensitized solar cells. *Journal of Power Sources*, *C*(351), 58–66.

Mabuchi, A., Tokumitsu, K., Fujimoto, H., & Kasuh, T. (1995). Charge-discharge characteristics of the mesocarbon miocrobeads heat-treated at different temperatures. *Journal of The Electrochemical Society*, *142*(4), 1041–1046.

May, G. J., Davidson, A., & Monahov, B. (2018). Lead batteries for utility energy storage: A review. *Journal of Energy Storage*, *15*, 145–157.

McAllister, M. J., Li, J. L., Adamson, D. H., Schniepp, H. C., Abdala, A. A., Liu, J., Herrera-Alonso, M., Milius, D. L., Car, R., Prud'homme, R. K., & Aksay, I. A. (2007). Single sheet functionalized graphene by oxidation and thermal expansion of graphite. *Chemistry of Materials*, *19*(18), 4396–4404.

McDowell, M. T., Lee, S. W., Nix, W. D., & Cui, Y. (2013). 25th anniversary article: Understanding the lithiation of silicon and other alloying anodes for lithium-ion batteries. *Advanced Materials*, *25*(36), 4966–4985.

Miao, F., Wijeratne, S., Zhang, Y., Coskun, U. C., Bao, W., & Lau, C. N. (2007). Phase-coherent transport in graphene quantum billiards. *Science*, *317*(5844), 1530–1533.

Monajjemi, M. (2017). Liquid-phase exfoliation (LPE) of graphite towards graphene: An ab initio study. *Journal of Molecular Liquids*, *C*(230), 461–472.

Mukherjee, R., Thomas, A. V., Krishnamurthy, A., & Koratkar, N. (2012). Photothermally reduced graphene as high-power anodes for lithium-ion batteries. *ACS Nano*, *6*(9), 7867–7878.

Muñoz, R., & Gómez-Aleixandre, C. (2013). Review of CVD synthesis of graphene. *Chemical Vapor Deposition*, *19*(10-11–12), 297–322.

Munuera, J. M., Paredes, J. I., Villar-Rodil, S., Ayán-Varela, M., Martínez-Alonso, A., & Tascón, J. M. D. (2016). Electrolytic exfoliation of graphite in water with multifunctional electrolytes: En route towards high quality, oxide-free graphene flakes. *Nanoscale*, *8*(5), 2982–2998.

Nair, R. R., Blake, P., Grigorenko, A. N., Novoselov, K. S., Booth, T. J., Stauber, T., Peres, N. M. R., & Geim, A. K. (2008). Fine structure constant defines visual transparency of graphene. *Science (New York, N.Y.)*, *320*(5881), 1308.

Nelson, P. A., Ahmed, S., Gallagher, K. G., & Dees, D. W. (2019). *Modeling the Performance and Cost of Lithium-Ion Batteries for Electric-Drive Vehicles* (Third Edition). Argonne, IL (United States): Argonne National Lab. (ANL).

Neudecker, B. J., Zuhr, R. A., & Bates, J. B. (1999). Lithium silicon tin oxynitride (LiySiTON): High-performance anode in thin-film lithium-ion batteries for microelectronics. *Journal of Power Sources*, *81–82*, 27–32.

Nitta, N., Wu, F., Lee, J. T., & Yushin, G. (2015). Li-ion battery materials: present and future. *Materials Today*, *18*(5), 252–264.

Novoselov, K. S., Geim, A. K., Morozov, S. v., Jiang, D., Zhang, Y., Dubonos, S. v., Grigorieva, I. v., & Firsov, A. A. (2004). Electric field in atomically thin carbon films. *Science*, *306*(5696), 666–669.

Orsini, F., du Pasquier, A., Beaudouin, B., Tarascon, J. M., Trentin, M., Langenhuizen, N., de Beer, E., & Notten, P. (1999). In situ SEM study of the interfaces in plastic lithium cells. *Journal of Power Sources*, *81–82*, 918–921.

Othman, N. H., Ismail, M. C., Mustapha, M., Sallih, N., Kee, K. E., & Jaal, R. A. (2019). Graphene-based polymer nanocomposites as barrier coatings for corrosion protection. *Progress in Organic Coatings*, *135*, 82-99.

Pacala, S., & Socolow, R. (2004). Stabilization wedges: solving the climate problem for the next 50 years with current technologies. *Science (New York, N.Y.)*, *305*(5686), 968–972.

Padhi, A. K., Nanjundaswamy, K. S., & Goodenough, J. B. (1997). Phospho-olivines as positive-electrode materials for rechargeable lithium batteries. *Journal of The Electrochemical Society*, *144*(4), 1188–1194.

Paek, S. M., Yoo, E. J., & Honma, I. (2009). Enhanced cyclic performance and lithium storage capacity of SnO2/graphene nanoporous electrodes with three-dimensionally delaminated flexible structure. *Nano Letters*, *9*(1), 72–75.

Pan, D., Feng, C., Wang, L., Liu, Y., Chen, Z., Shi, W., & Li, Z. (2016). Binder-free graphene organogels as cost-efficient counter electrodes for dye-sensitized solar cells. *Electrochimica Acta*, *191*, 946–953.

Park, S., & Ruoff, R. S. (2009). Chemical methods for the production of graphenes. *Nature Nanotechnology, 4*(4), 217–224.

PbSO, P., Koh, N., -, -e, Li Si, V., & LiX, S. (2008). Building better batteries. *Nature*, *451*(7179), 652–657.

Pender, J. P., Jha, G., Youn, D. H., Ziegler, J. M., Andoni, I., Choi, E. J., Heller, A., Dunn, B. S., Weiss, P. S., Penner, R. M., & Mullins, C. B. (2020). Electrode degradation in lithium-ion batteries. *ACS Nano*, *14*(2), 1243–1295.

Peres, N. M. R., Castro Neto, A. H., & Guinea, F. (2006). Conductance quantization in mesoscopic graphene. *Physical Review B - Condensed Matter and Materials Physics*, *73*(19), 195411.

Petnikota, S., Rotte, N. K., Srikanth, V. V. S. S., Kota, B. S. R., Reddy, M. v., Loh, K. P., & Chowdari, B. V. R. (2014). Electrochemical studies of few-layered graphene as an anode material for Li ion batteries. *Journal of Solid State Electrochemistry*, *4*(18), 941–949.

Rand, D. A. J., & Moseley, P. T. (2009). Secondary batteries – lead– acid systems: Overview. *Encyclopedia of Electrochemical Power Sources*, 550–575.

Ravet, N., Chouinard, Y., Magnan, J. F., Besner, S., Gauthier, M., & Armand, M. (2001). Electroactivity of natural and synthetic triphylite. *Journal of Power Sources*, *97–98*, 503–507.

Redondo-Obispo, C., Ripolles, T. S., Cortijo-Campos, S., Álvarez, A. L., Climent-Pascual, E., de Andrés, A., & Coya, C. (2020). Enhanced stability and efficiency in inverted perovskite solar cells through graphene doping of PEDOT:PSS hole transport layer. *Materials & Design*, *191*, 108587.

Reina, A., Jia, X., Ho, J., Nezich, D., Son, H., Bulovic, V., Dresselhaus, M. S., & Jing, K. (2009). Large area, few-layer graphene films on arbitrary substrates by chemical vapor deposition. *Nano Letters*, *9*(1), 30–35.

Reina, A., Thiele, S., Jia, X., Bhaviripudi, S., Dresselhaus, M. S., Schaefer, J. A., & Kong, J. (2010). Growth of large-area single- and Bi-layer graphene by controlled carbon precipitation on polycrystalline Ni surfaces. *Nano Research*, *2*(6), 509–516.

Rossen, E., Jones, C. D. W., & Dahn, J. R. (1992). Structure and electrochemistry of LixMnyNi1−yO2. *Solid State Ionics*, *57*(3–4), 311–318.

Ruland, W. (2004). X-ray studies on preferred orientation in carbon fibers. *Journal of Applied Physics*, *38*(9), 3585.

Sang, B., Li, Z. wei, Li, X. hong, Yu, L. gui, & Zhang, Z. jun. (2016). Graphene-based flame retardants: a review. *Journal of Materials Science*, *51*(18), 8271–8295.

Schmidt-Rohr, K. (2018). How batteries store and release energy: Explaining basic electrochemistry. *Journal of Chemical Education*, *95*(10), 1801–1810.

Shukla, A. K., & Prem Kumar, T. (2008). Materials for next-generation lithium batteries. *Current science*, *94*(3), 314-331.

Sinclair, R. C., Suter, J. L., & Coveney, P. v. (2019). Micromechanical exfoliation of graphene on the atomistic scale. *Physical Chemistry Chemical Physics*, *21*(10), 5716–5722.

Song, H. S., Li, S. L., Miyazaki, H., Sato, S., Hayashi, K., Yamada, A., & Tsukagoshi, K. (2012). Origin of the relatively low transport mobility of graphene grown through chemical vapor deposition. *Scientific reports*, *2*(1), 1-6.

Speirs, J., Contestabile, M., Houari, Y., & Gross, R. (2014). The future of lithium availability for electric vehicle batteries. *Renewable and Sustainable Energy Reviews*, *35*, 183–193.

Stankovich, S., Dikin, D. A., Dommett, G. H. B., Kohlhaas, K. M., Zimney, E. J., Stach, E. A., Piner, R. D., Nguyen, S. B. T., & Ruoff, R. S. (2006). Graphene-based composite materials. *Nature*, *442*(7100), 282–286.

Sun, X., Liu, Z., Welsher, K., Robinson, J. T., Goodwin, A., Zaric, S., & Dai, H. (2008). Nano-graphene oxide for cellular imaging and drug delivery. *Nano Research*, *1*(3), 203–212.

Sun, Y., Tang, J., Zhang, K., Yuan, J., Li, J., Zhu, D. M., Ozawa, K., & Qin, L. C. (2017). Comparison of reduction products from graphite oxide and graphene oxide for anode applications in lithium-ion batteries and sodium-ion batteries. *Nanoscale*, *9*(7), 2585–2595.

Sutter, P. W., Flege, J. I., & Sutter, E. A. (2008). Epitaxial graphene on ruthenium. *Nature Materials*, *7*(5), 406–411.

Syama, S., & Mohanan, P. v. (2019). Comprehensive application of graphene: emphasis on biomedical concerns. *Nano-Micro Letters, 11*(1), 1–31.

Tarascon, J. M. (2010). Key challenges in future li-battery research. *Philosophical Transactions of the Royal Society A: Mathematical, Physical and Engineering Sciences*, *368*(1923), 3227–3241.

Tarascon, J. M., & Armand, M. (2001). Issues and challenges facing rechargeable lithium batteries. *Nature 2001*, *414*(6861), 359–367.

Thackeray, M. M., David, W. I. F., Bruce, P. G., & Goodenough, J. B. (1983). Lithium insertion into manganese spinels. *Materials Research Bulletin*, *18*(4), 461–472.

Thackeray, M. M., Johnson, C. S., Vaughey, J. T., Li, N., & Hackney, S. A. (2005). Advances in manganese-oxide 'composite' electrodes for lithium-ion batteries. *Journal of Materials Chemistry*, *15*(23), 2257–2267.

Viculis, L. H., Mack, J. J., & Kaner, R. B. (2003). A chemical route to carbon nanoscrolls. *Science (New York, N.Y.)*, *299*(5611), 1361.

Vikström, H., Davidsson, S., & Höök, M. (2013). Lithium availability and future production outlooks. *Applied Energy*, *110*, 252–266.

Wang, G., Shen, X., Yao, J., & Park, J. (2009). Graphene nanosheets for enhanced lithium storage in lithium ion batteries. *Carbon*, *47*(8), 2049–2053.

Wang, G., Wang, B., Park, J., Wang, Y., Sun, B., & Yao, J. (2009). Highly efficient and large-scale synthesis of graphene by electrolytic exfoliation. *Carbon*, *47*(14), 3242–3246.

Wang, R., Han, M., Zhao, Q., Ren, Z., Guo, X., Xu, C., Hu, N., & Lu, L. (2017). Hydrothermal synthesis of nanostructured graphene/polyaniline composites as high-capacitance electrode materials for supercapacitors. *Scientific Reports*, *7*(1), 1–9.

Wang, W., & Kumta, P. N. (2010). Nanostructured hybrid silicon/carbon nanotube heterostructures: Reversible high-capacity lithium-ion anodes. *ACS Nano*, *4*(4), 2233–2241.

Wang, X., Lu, X., Liu, B., Chen, D., Tong, Y., & Shen, G. (2014). Flexible energy-storage devices: design consideration and recent progress. *Advanced Materials, 26*(28), 4763–4782.

Wang, Y., Gao, S., Xu, W., Wang, Z., Wang, Y., Gao, S., Xu, W., & Wang, Z. (2020). Nanogenerators with superwetting surfaces for harvesting water/liquid energy. *Advanced Functional Materials*, *30*(26), 1908252.

Wang, Y., Li, Z., Wang, J., Li, J., & Lin, Y. (2011). Graphene and graphene oxide: biofunctionalization and applications in biotechnology. *Trends in Biotechnology*, *29*(5), 205–212.

Wang, Z., & Liu, C. J. (2015). Preparation and application of iron oxide/graphene based composites for electrochemical energy storage and energy conversion devices: Current status and perspective. *Nano Energy*, *11*, 277–293.

Wu, J. bin, Lin, M. L., Cong, X., Liu, H. N., & Tan, P. H. (2018). Raman spectroscopy of graphene-based materials and its applications in related devices. *Chemical Society Reviews*, *47*(5), 1822–1873.

Wu, Q., Xu, Y., Yao, Z., Liu, A., & Shi, G. (2010). Supercapacitors based on flexible graphene/polyaniline nanofiber composite films. *ACS Nano*, *4*(4), 1963–1970.

Xie, K., & Wei, B. (2014). Materials and structures for stretchable energy storage and conversion devices. *Advanced Materials*, *26*(22), 3592–3617.

Xin, G., Hwang, W., Kim, N., Cho, S. M., & Chae, H. (2010). A graphene sheet exfoliated with microwave irradiation and interlinked by carbon nanotubes for high-performance transparent flexible electrodes. *Nanotechnology*, *21*(40), 405201.

Xu, C., Xu, B., Gu, Y., Xiong, Z., Sun, J., & Zhao, X. S. (2013). Graphene-based electrodes for electrochemical energy storage. *Energy & Environmental Science*, *6*(5), 1388–1414.

Xu, K. (2004). Nonaqueous liquid electrolytes for lithium-based rechargeable batteries. *Chemical Reviews*, *104*(10), 4303–4417.

Yadav, R., Tirumali, M., Wang, X., Naebe, M., & Kandasubramanian, B. (2020). Polymer composite for antistatic application in aerospace. *Defence Technology*, *16*(1), 107–118.

Yamada, A., Chung, S. C., & Hinokuma, K. (2001). Optimized LiFePO4 for lithium battery cathodes. *Journal of The Electrochemical Society*, *148*(3), A224.

Yoo, E., & Zhou, H. (2011). Li-air rechargeable battery based on metal-free graphene nanosheet catalysts. *ACS Nano*, *5*(4), 3020–3026.

Zhang, J., Zhang, L., Sun, F., & Wang, Z. (2018). An overview on thermal safety issues of lithium-ion batteries for electric vehicle application. *Ieee Access*, *6*, 23848-23863.

Zhang, W.-J., Zhang, & Wei-Jun. (2011). A review of the electrochemical performance of alloy anodes for lithium-ion batteries. *JPS*, *196*(1), 13–24.

Zhou, G., Li, F., & Cheng, H. M. (2014). Progress in flexible lithium batteries and future prospects. *Energy & Environmental Science*, *7*(4), 1307–1338.